IP_3 mediated global Ca^{2+} signals arise through two temporally and spatially distinct modes of Ca^{2+} release

Jeffrey T. Lock[1] and Ian Parker [1,2]

[1]Department of Neurobiology & Behavior, UC Irvine, Irvine, CA.

[2]Department of Physiology & Biophysics, UC Irvine, Irvine, CA.

Address correspondence to:

Jeffrey T. Lock
Department of Neurobiology and Behavior
University of California,
Irvine, CA92697
lockj@uci.edu

Running title: *Punctate and diffuse modes of Ca^{2+} liberation via IP_3Rs*

SUMMARY

The 'building-block' model of inositol trisphosphate (IP_3)-mediated Ca^{2+} liberation posits that cell-wide cytosolic Ca^{2+} signals arise through coordinated activation of localized Ca^{2+} puffs generated by stationary clusters of IP_3 receptors (IP_3Rs). Here, we revise this hypothesis, applying fluctuation analysis to resolve Ca^{2+} signals otherwise obscured during large Ca^{2+} elevations. We find the rising phase of global Ca^{2+} signals is punctuated by a flurry of puffs, which terminate before the peak by a mechanism involving partial ER Ca^{2+} depletion. The continuing rise in Ca^{2+}, and persistence of global signals even when puffs are absent, reveal a second mode of spatiotemporally diffuse Ca^{2+} signaling. Puffs make only small, transient contributions to global Ca^{2+} signals, which are sustained by diffuse release of Ca^{2+} through a functionally distinct process. These two modes of IP_3-mediated Ca^{2+} liberation have important implications for downstream signaling, imparting spatial and kinetic specificity to Ca^{2+}-dependent effector functions and Ca^{2+} transport.

INTRODUCTION

Cytosolic Ca^{2+} signals generated by the liberation of Ca^{2+} ions sequestered in the endoplasmic reticulum (ER) through inositol trisphosphate receptor (IP_3R) channels regulate ubiquitous cellular processes as diverse as gene transcription, secretion, mitochondrial energetics, electrical excitability and fertilization[1,2]. Cells achieve such unique repertories of Ca^{2+}-dependent functions by generating a hierarchy of cytosolic Ca^{2+} signals with markedly different spatial scales and temporal durations, ranging from brief, localized Ca^{2+} transients called puffs[3,4] to larger and more prolonged Ca^{2+} elevations that engulf the cell. Global elevations in cytosolic Ca^{2+} typically last several seconds and may appear as waves that propagate throughout the cell[5]. They can recur as oscillations with periods between a few seconds and a few minutes, and are thought to encode information in a 'digital' manner, whereby increasing stimulus strength results predominantly in an increase in frequency rather than amplitude[6,7]. Puffs, on the other hand, are tightly localized elevations in cytosolic Ca^{2+} generated by stationary clusters containing small numbers of IP_3Rs, which last only tens or a few hundreds of milliseconds and remain restricted within a few micrometers[8,9].

The patterning of cellular Ca^{2+} signals evoked by IP_3 is largely determined by the functional properties of the IP_3Rs and by their spatial arrangement in the ER membrane. Crucially, the opening of IP_3R channels is regulated by cytosolic Ca^{2+} itself, in addition to IP_3. Low concentrations of Ca^{2+} increase the open probability of the channel whereas high concentrations favor a closed state[10–12]. This biphasic

modulation of IP_3Rs by Ca^{2+} leads to the phenomenon of Ca^{2+}-induced Ca^{2+} release (CICR). Ca^{2+} diffusing from one open channel may thus trigger the opening of adjacent channels, with self-reinforcing CICR countered by Ca^{2+} feedback inhibition. The clustered distribution of IP_3Rs further shapes the extent of this regenerative process. CICR may remain locally restricted to a single cluster, containing from a few to a few tens of functional IP_3Rs, to produce a puff; whereas it is proposed that a global response is generated by successive cycles of CICR and Ca^{2+} diffusion acting over longer spatial ranges to recruit successive puff sites[8,9,13–18]. However, the transition between these modes remains an area of active investigation[19–23], and recent theoretical simulations have questioned whether Ca^{2+} released through puff activity is alone sufficient to propagate global cytosolic Ca^{2+} signals[24].

Here, we examined the nature of Ca^{2+} liberation through IP_3Rs during global cellular Ca^{2+} signals, asking whether this accords with the widely-accepted 'building block' model[8,9,13,14,17,18,25] in which global signals are constructed by the summation of coordinated, pulsatile activation of Ca^{2+} release at puff sites; or whether global signals also involve an additional mode of Ca^{2+} liberation that is more homogeneous in space and time. Although Ca^{2+} puffs are often evident during the initial rising phase of global Ca^{2+} signals[8,14,17,18], a challenge in answering this question arises because puffs become obscured as the overall cytosolic Ca^{2+} level continues to increase. To reveal and monitor temporally rapid and spatially confined Ca^{2+} transients (puffs) during even large amplitude global Ca^{2+} elevations we developed image processing and analysis routines to analyze local fluctuations in Ca^{2+}

fluorescence signals[26]. We applied these routines to Ca^{2+} recordings obtained both by total internal reflection fluorescence (TIRF) microscopy to resolve signals arising near the plasma membrane, and by lattice light-sheet (LLS) microscopy to acquire optical sections through the cell interior. We find that rapid flurries of Ca^{2+} puffs accompany the rising phase of global Ca^{2+} signals evoked by photoreleased IP_3 and by agonist stimulation of the IP_3 signaling pathway, but these rapidly terminate before the peak of the response through a mechanism regulated by ER Ca^{2+} store content. The punctate liberation of Ca^{2+} via transient, localized Ca^{2+} puffs contributes only a small fraction of the total Ca^{2+} liberated during global Ca^{2+} signals, which are instead sustained by diffuse Ca^{2+} liberation through a functionally distinct mode of release. These two modes of IP_3-mediated Ca^{2+} release will likely selectively activate different populations of effectors; those positioned close to the IP_3R clusters that mediate puffs and which respond to brief, repetitive transients of $[Ca^{2+}]$, and others that respond to a more sustained, spatially diffuse elevation of bulk cytosolic $[Ca^{2+}]$.

RESULTS

Fluctuation processing of Ca^{2+} images highlights transient signals.

Our central question was whether IP_3-evoked Ca^{2+} liberation during cell-wide Ca^{2+} signals arises through coordinated activation of pulsatile, spatially-localized events, analogous to the local Ca^{2+} puffs observed with weaker IP_3 stimulation or after loading cells with EGTA to suppress global signals[27,28]. To better visualize and

identify transient, localized Ca^{2+} events occurring during the course of larger, global elevations of Ca^{2+}, we developed an image processing algorithm to highlight and quantify temporal fluctuations of the Ca^{2+} fluorescence signal. We previously described the use of pixel-by-pixel power spectrum analysis of temporal Ca^{2+} fluctuations for this purpose[29], but this is computationally intensive and unfeasible for large data sets. Here we adopted a faster approximation, by first temporally band-pass filtering image stacks and then calculating the standard deviation (SD) of the fluorescence fluctuations at each pixel over a running time window[26].

The conceptual basis of the algorithm is illustrated in Figure 1 (see also Movie M1). WT HEK293 cells were loaded with the fluorescent Ca^{2+} indicator Cal520 and imaged by TIRF microscopy during global cytosolic Ca^{2+} signals. The panels in Fig. 1A show Cal520 fluorescence of individual image frames of a HEK cell captured before (i) and after (ii-v) photorelease of i-IP_3, an active, metabolically stable analog of IP_3. Photoreleased i-IP_3 evoked a widespread increase in fluorescence throughout the cell that peaked within about 5 s, during which time several transient, local 'hot spots' were evident. These are visible in Movie M1, but are not readily apparent in Fig. 1A because of the extended grey scale required to encompass the peak global fluorescence signal. To illustrate the activity at local hot spots we monitored fluorescence from regions of interest (ROIs) centered on 24 sites (Fig. 1C). Traces from these sites showed progressive, large fluorescence increases above the baseline, with small, superimposed transients (puffs) during the rising phase. To better discriminate these localized signals, we high-pass (1 Hz)

filtered the image stack, pixel-by-pixel, to strip out the slow increase in global fluorescence. Fig. 1D shows mean power spectra averaged from the 24 sites during image sequences (5s) acquired before (control; blue trace) and immediately following (red trace) photorelease of i-IP_3. The control, baseline spectrum showed substantially uniform power across all frequencies above the applied 1 Hz high-pass filter, compatible with the dominant noise source arising from 'white' photon shot noise. Strikingly, the spectrum obtained during the rise of the global Ca^{2+} signal showed much greater power at frequencies between about 1 - 20 Hz as compared to the control spectrum, rolling off at higher frequencies to a noise floor determined by photon shot noise. We thus developed an approach to isolate the low-frequency fluctuations attributable to transient Ca^{2+} puffs, while subtracting the photon shot noise that would arise in linear proportion to the overall fluorescence intensity.

Beginning with a black level-subtracted 'raw' fluorescence image stack, our algorithm applied a spatial filter (Gaussian blur with sigma ~1 μm), and a band-pass temporal Butterworth filter (3-20 Hz). The resulting image stack was then processed by a running boxcar window (160 ms) that, for each pixel, calculated the standard deviation (SD) of the fluorescence signal at that pixel throughout the duration of the window. These parameters were chosen to optimally 'tune' the algorithm to reject slow changes in baseline fluorescence and attenuate high frequency photon shot noise while retaining frequencies resulting from puff activity (Supplemental fig. S1). Lastly, the algorithm corrected for photon shot noise by subtracting a scaled measure of the square root of fluorescence intensity at each

pixel. If measurements were in terms of numbers of detected photons, the SD would equal the square root of the intensity; however, that was not the case for our records because of considerations including the camera conversion factor and the filtering applied to the image stack. We thus empirically determined an appropriate scaling factor, by determining the linear slope of a plot of mean variance *vs.* mean fluorescence emission from a sample of fluorescein where photon shot noise was expected to be the major noise source (Supplemental fig. S2).

Fig. 1B presents representative SD images calculated by the algorithm, at time points corresponding to the panels in Fig. 1A, and Supplemental movie M1 shows fluorescence and SD images throughout the response. The SD signal was uniformly close to zero throughout the cell before stimulation (Fig. 1B, panel i), while discrete, transient hot spots were clearly evident at several different sites during the rising phase of the global Ca^{2+} elevation (panels ii-iv), but ceased at the time of the peak response (panel v). This behavior is further illustrated by the black traces in Fig. 1E, showing overlaid SD measurements from the 24 hot spots of activity. A flurry of transient events at these sites peaked during the rising phase of the global Ca^{2+} response to photoreleased i-IP_3 but had largely subsided by the time of the maximal global Ca^{2+} elevation. Even though the global Ca^{2+} level then stayed elevated for many seconds the mean SD signals at these regions remained low. Measurement of the SD signal derived from a ROI encompassing the entire cell (yellow trace, Fig. 1E) closely tracked the aggregate kinetics of the individual puff sites.

To further validate the fluctuation analysis algorithm, we examined a situation where cytosolic [Ca^{2+}] was expected to rise in a smoothly graded manner, without overt temporal fluctuations or spatial heterogeneities. For this, we imaged Cal520 fluorescence by TIRF microscopy in HEK293 3KO cells in which all IP_3R isoforms were knocked out[30]. We pipetted an aliquot of ionomycin (10 μl of 10 μM) into the 2.5 ml volume of Ca^{2+}-free bathing solution at a distance from the cell chosen so that the diffusion of ionomycin evoked a slow liberation of Ca^{2+} from intracellular stores to give a fluorescence signal of similar amplitude (8.3 $\Delta F/F_0$) and kinetics to that evoked by photoreleased i-IP_3 (6.9 $\Delta F/F_0$) in Fig. 1A,C. Fig. 1F shows snapshots of 'raw' fluorescence captured before (i) and during (ii-v) application of ionomycin. The fluorescence rose uniformly throughout the cell without any evident hot spots of local transients in the SD images (Fig. 1G and supplemental movie M1). Measurements from 24 randomly located ROIs (squares in Fig. 1F) showed only smooth rises in fluorescence (Fig. 1H). Mean spectra from these regions (Fig. 1I) displayed flat, substantially uniform distributions of power across all frequencies, consistent with photon shot noise increasing in proportion to the mean fluorescence level. Notably, SD signals from local ROIs (Fig. 1J, superimposed black traces) and from a ROI encompassing the entire cell (yellow trace) showed no increase in fluctuations beyond that expected for photon shot noise.

Temporal fluctuations reflect spatially localized Ca^{2+} signals.

The SD image stacks generated by the temporal fluctuation algorithm showed transient hot spots of Ca^{2+} release associated with temporal fluctuations. However,

the SD signal could also include temporal fluctuations in fluorescence that were spatially blurred or uniform across the cell. To determine whether these contribute appreciably, or whether the SD signal could be taken as a good reporter of localized puff activity, we developed a second algorithm to reveal spatial Ca^{2+} variations in Cal520 fluorescence image stacks (Supplemental fig. S3).

Ca^{2+} image stacks were first temporally bandpass filtered as described above. The algorithm then calculated, frame by frame, the difference between strong and weak Gaussian blur functions (respective standard deviations of about 4 and 1 μm at the specimen), essentially acting as a spatial bandpass filter to attenuate high spatial frequencies caused by pixel-to-pixel shot noise variations and low frequency variations resulting from the spread of Ca^{2+} waves across the cell, while retaining spatial frequencies corresponding to the spread of local Ca^{2+} puffs. The resulting spatial SD images were remarkably similar to images generated by the temporal fluctuation analysis routine (Supplemental fig. S3A), and traces of mean cell-wide temporal and spatial SD signals during Ca^{2+} elevations matched closely (Supplemental figs. S3B-E). We thus conclude that the temporal SD signals faithfully reflect transient, localized Ca^{2+} puff activity while minimizing confounding contributions from shot noise and slower changes in global fluorescence.

Fluctuation analysis reveals a transient flurry of puffs during global Ca^{2+} signals.

In Fig. 1 we show traces from discrete subcellular regions to illustrate how temporal SD images detect transient, local Ca^{2+} elevations while being insensitive to homogeneous global Ca^{2+} elevations. However, for all the following experiments in this paper we show SD signals derived from single ROIs that completely encompassed each cell, so as to obtain an aggregate measure of puff activity throughout the cell and obviate any subjective bias that might arise in selecting smaller, sub-cellular regions. Unless otherwise stated, all imaging was done by TIRF microscopy with cells bathed in a zero Ca^{2+} solution including 300 μM EGTA to avoid possible complication from entry of extracellular Ca^{2+} into the cytosol.

Fig. 2 and supplemental movies M2-M3 present records from WT HEK cells loaded with Cal520 and caged i-IP_3 showing how the SD signal reveals the patterns of puff activity underlying global Ca^{2+} signals. Under basal conditions the shot noise-corrected cell-wide SD signals were almost flat, with a mean around zero (Fig. 2A, movie M2), indicating a negligible level of local Ca^{2+} activity at rest. Photorelease of small amounts of i-IP_3 by brief (~100 ms) UV flashes evoked Ca^{2+} puffs - directly visible in the Cal520 fluorescence ratio movie M2, and more evident as sharp transients in the whole-cell SD trace - but without generating any appreciable global rise in basal Ca^{2+} (Fig. 2B). Longer flashes (200-1000 ms) generated whole-cell elevations in cytosolic Ca^{2+} that rose and fell over several seconds, with fluorescence signals reaching peak amplitudes in rough proportion to the flash duration (smooth traces, Fig. 2C-E; movies M3). SD movies (M3) and whole-cell SD traces (noisy traces, Fig. 2C-E) revealed an underlying flurry of localized, transient

Ca^{2+} events during the rising phase of the global Ca^{2+} responses. In instances where global Ca^{2+} signals were small and slowly rising, the SD traces showed Ca^{2+} transients persisting throughout the prolonged rising phase (Fig. 2C). On the other hand, the SD traces from cells exhibiting intermediate (Fig. 2D) and fast rising (Fig. 2E) global signals revealed Ca^{2+} fluctuations that began almost immediately following photorelease of i-IP_3, reached a maximum during the rising phase of the global signal, but then declined almost to baseline by the peak of the response.

The records in Fig. 2A-E and movies M2, M3 illustrate representative responses in individual cells. To pool data from multiple cells we grouped records into categories matching the examples in Fig. 2B-E: i.e., responses showing puffs without an appreciable elevation of global Ca^{2+}; and slow-, intermediate- and fast- rising global Ca^{2+} responses. Fig. 2G shows overlaid traces depicting the mean Cal520 fluorescence ratios ($\Delta F/F_0$) of the global Ca^{2+} responses from cells in these different categories, and Fig. 2H shows the associated mean SD traces. Notably, in all three categories where global Ca^{2+} signals were evoked (Fig. 2C-E) the mean SD signals were transient, indicating that puff activity was largely confined to the rising phase of the global Ca^{2+} elevation and largely ceased by the time the global signal reached a maximum. The durations of the puff flurries progressively shortened with increasing rates of rise in global Ca^{2+} and the magnitudes of the SD signal at the peak of the flurry activity increased.

Ca^{2+} signals evoked by agonist activation and photoreleased i-IP_3 show similar patterns of puff activity.

UV photorelease of i-IP_3 provides a convenient tool to activate IP_3Rs with precise timing and control of the amount released. However, this IP_3 analog is slowly metabolized by the cell, remaining elevated for minutes following photo-uncaging[28,31], and its uniform release throughout the cell differs from endogenous generation of IP_3 at the cell membrane[32,33]. We thus compared responses evoked by photoreleased i-IP_3 with those activated by the G-protein coupled muscarinic receptor agonist carbachol (CCH), locally applied through a picospritzer-driven micropipette (puffer pipet) positioned above WT HEK cells bathed in zero Ca^{2+} medium. A brief (5 s) pulse of CCH elicited a rapid, global rise in Ca^{2+} that was accompanied by an underlying burst of local Ca^{2+} signals (Fig. 2F; supplemental movie M4). As with responses evoked by photoreleased i-IP_3, fluctuations arising from local Ca^{2+} signals occurred predominantly during the initial portion of the rising phase and then subsided to near basal levels before the peak of the global response. Fig. 2I shows mean traces of whole-cell global Ca^{2+} signals ($\Delta F/F_0$) and SD signals of CCH-evoked responses from 12 cells. Peak fluorescence amplitudes were similar to mean values for 11 cells stimulated by strong photorelease of i-IP_3 ($\Delta F/F_0$ of 8.89 ± 0.3 for CCH vs. 7.27 ± 0.4 for i-IP_3); as were the rising phase kinetics of the global Ca^{2+} signal (rise from 20% to 80% of peak 0.70 s ± 0.05 s for CCH vs. 0.80 s ± 0.06 s for i-IP_3). However, global Ca^{2+} elevations evoked by CCH decayed more rapidly than those evoked by i-IP_3 (fall from 80% to 20% of peak 6.33 s ± 0.3 s for

CCH vs 20.05 s ± 3.2 s for i-IP_3) - likely because the slowly-degraded i-IP_3 evoked a more sustained release of Ca^{2+}.

Ca^{2+} puff activity terminates during the rising phase of global Ca^{2+} signals.

Puff activity (SD signal) showed a characteristic rise and fall during the rising phase of global Ca^{2+} signals, and both parameters accelerated with increasing photorelease of i-IP_3 (Fig. 2). To investigate the relationship between the bulk Ca^{2+} level and puff activity in a time-independent manner we took paired measurements of cell-wide SD signals and Ca^{2+} level ($\Delta F/F_0$) at intervals during the rising phase of IP_3-evoked Ca^{2+} elevations. Fig. 3A shows a scatter plot of SD vs. $\Delta F/F_0$ values for measurements from the cell in Fig. 2D, and Fig. 3B plots corresponding mean data pooled from groups of cells that gave i-IP_3-evoked global signals with fast (pink circles), intermediate (green triangles) and slow (blue squares) rising phases. Although the amplitudes of the SD signals were greater for the faster rising responses, all cells showed similar 'inverted U' shaped relationships. In all three groups the SD signal was maximal when the Cal520 fluorescence ratio reached a $\Delta F/F_0$ value of about 2 and then declined progressively as global Ca^{2+} rose higher. This is illustrated more clearly in Fig. 3C, where the curves for the three groups of cells superimpose closely after normalization to the same peak SD level. A closely similar inverted U relationship was observed for Ca^{2+} elevations evoked by CCH (Fig. 3D).

The decline in SD signal at higher Ca^{2+} levels during global signals cannot be attributed to a failure of our algorithm to detect local fluctuations because of saturation of the Cal520 indicator dye. Notably, maximal fluorescence responses evoked by addition of ionomycin in high (10 mM) Ca^{2+}-containing medium ($\Delta F/F_0$ of 18.93 ± 1.5; n = 32 cells) considerably exceeded the peak fluorescence level evoked by even strong photorelease of i-IP_3 (mean $\Delta F/F_0$ 7.27 ± 0.4, n = 11 cells), and were greatly in excess of the fluorescence level ($\Delta F/F_0 \sim 2$; Fig. 3) at which the SD signal began to decline. Moreover, we observed instances of local Ca^{2+} signals even during large global Ca^{2+} elevations ($\Delta F/F_0 > 8$; Supplemental fig. S4), and obtained SD signals using the lower affinity indicator fluo8L (Kd 1.86 μM vs. 320 nM for Cal520) confirming that puff activity was similarly suppressed prior to the peak of i-IP_3 evoked Ca^2 elevations (Supplemental fig. S5).

Ca^{2+} puffs are independent of extracellular Ca^{2+}.

We performed the experiments in Figs. 1-3 using a bathing solution containing no added Ca^{2+} together with 300 μM EGTA to specifically monitor the release of Ca^{2+} from intracellular stores without possible confounding signals arising from entry of Ca^{2+} across the plasma membrane. To explore whether these results were representative of responses in more physiological conditions, we examined Ca^{2+} signals evoked by photoreleased i-IP_3 in WT HEK cells bathed in solutions containing 2 mM Ca^{2+} (Supplemental fig. S6). Cell-wide Ca^{2+} responses and flurries of local Ca^{2+} signals closely matched the patterns of activity in cells imaged in the

absence of extracellular Ca^{2+} (Supplemental fig. S6B-G), and scatter plots of SD signal vs. global Ca^{2+} fluorescence signal (Supplemental fig. S6H,I) mirrored those in the absence of extracellular Ca^{2+} (Fig. 3). Thus, the puff activity during IP_3-evoked global Ca^{2+} elevations appears independent of Ca^{2+} influx into the cell. However, global Ca^{2+} responses decayed more slowly when Ca^{2+} was included in the bath solution ($fall_{80-20}$ for strong photorelease of i-IP_3 35.87 s ± 3.9 s in 2 mM Ca^{2+} vs. 20.05 s ± 3.2 s in zero Ca^{2+}; $Fall_{80-20}$ for CCH of 13.06 s ± 0.5 s in 2 mM Ca^{2+} vs 6.33 s ± 0.3 in zero Ca^{2+}). A likely explanation is that influx through slowly activating store-operated channels prolongs the response when extracellular Ca^{2+} is present.

Patterns of Ca^{2+} release are largely unaffected by inhibition of mitochondrial and lysosomal Ca^{2+} uptake.

Mitochondria and lysosomes help shape intercellular Ca^{2+} dynamics by accumulating and releasing Ca^{2+}[34–37]. To examine whether activity of these organelles influenced the spatial-temporal occurrence of puffs during IP_3-evoked global Ca^{2+} signals, we treated WT HEK cells for 10 min with FCCP to inhibit mitochondrial[38,39] and lysosomal[40] Ca^{2+} uptake by dissipating the proton gradient necessary for Ca^{2+} flux. (Supplemental fig. S7A). Mean traces of whole-cell Ca^{2+} fluorescence ($\Delta F/F_0$) and associated SD fluctuations in FCCP-treated cells stimulated with CCH exhibited local and global Ca^{2+} signals similar to vehicle-treated controls, though with slightly smaller peak magnitudes (Supplemental fig. S7C-D). Scatter plots of SD signal vs. bulk Ca^{2+} level during the rising phase of CCH-evoked Ca^{2+}

elevations were closely similar in control and following FCCP application (Supplemental fig. S7E).

HeLa and HEK cells exhibit similar patterns of Ca^{2+} signals

We utilized HEK cells for most experiments because of the availability of cell lines expressing individual IP_3R isoforms[30]. The patterning of local, transient Ca^{2+} signals during IP_3-mediated whole-cell Ca^{2+} elevations was not unique to this cell type. Stimulation of HeLa cells with histamine also evoked global Ca^{2+} signals accompanied by flurries of local Ca^{2+} activity during the rising phase, which subsided as Ca^{2+} levels continued to rise (supplemental fig. S8).

Ca^{2+} puffs do not terminate because of rising cytosolic Ca^{2+} during cell-wide elevations.

In light of the resemblance between the inverted U relationship between puff activity and Ca^{2+} level (Fig. 3) and the well-known bell-shaped curve for biphasic modulation of IP_3R channel activation by Ca^{2+}[11,12] we considered whether the suppression of puff activity during global elevations might result because IP_3Rs became inhibited by rising cytosolic Ca^{2+} levels. To test this, we first examined the effect of elevating cytosolic Ca^{2+} levels prior to evoking IP_3-mediated Ca^{2+} signals. We loaded HEK WT cells with caged Ca^{2+} (NP-EGTA) and delivered photolysis flashes of varying durations to cause jumps of cytosolic free Ca^{2+} of different magnitudes before locally applying CCH from a puffer pipette (Fig. 4A). Although the SD signals evoked by CCH declined progressively with increasing prior photorelease

404 of Ca^{2+}, this reduction was matched by a similar diminution in peak amplitudes
405 ($\Delta F/F_0$) of the global Ca^{2+} signal. The open symbols in Fig. 4B plot the ratio of puff
406 activity (integral under SD traces) relative to the size of the CCH-evoked global Ca^{2+}
407 signal in each cell, and are presented after binning according to the magnitude of the
408 preceding Ca^{2+} jump evoked by photolysis of caged Ca^{2+}. Mean ratios (Fig. 4B, filled
409 symbols) remained almost constant for all Ca^{2+} jumps; even at levels ($\Delta F/F_0$ >6)
410 corresponding to those where puff activity was strongly suppressed during the
411 rising phase of global responses (Fig. 3).
412
413 As a complementary approach, we then examined the effect of buffering the rise in
414 cytosolic [Ca^{2+}] during global responses by strong cytosolic loading of EGTA.
415 Fig. 4C shows representative SD and $\Delta F/F_0$ traces in response to photoreleased i-IP_3
416 from a WT HEK cell that was loaded with EGTA by incubation for 1 hr with 15 μM
417 EGTA-AM. The cell showed a typical flurry of puff activity like that in non EGTA-
418 loaded cells. Puffs ceased before the peak of the global Ca^{2+} signal, even though the
419 amplitude of the signal (2.5 $\Delta F/F_0$) was strongly attenuated. Fig. 4D summarizes
420 mean data from multiple cells, plotting paired measurements of cell-wide SD signals
421 and Ca^{2+} level ($\Delta F/F_0$) at intervals during the rising phase of IP_3-evoked Ca^{2+}
422 elevations, as in Fig. 3. The data again followed an inverted U relationship (solid
423 circles), but in comparison to control, non EGTA-loaded cells (open circles) the
424 relationship was shifted markedly to the left. Notably, the peak SD signal was
425 attained at a fluorescence level of about 0.40 $\Delta F/F_0$ vs. about 2 $\Delta F/F_0$ for controls,

and puffs were substantially suppressed at fluorescence levels ($\Delta F/F_0$ ~2) where the puff activity was near maximal in control cells.

Taken together, these results demonstrate that inhibition of IP_3Rs by elevated cytosolic [Ca^{2+}] is not the primary mechanism causing puff activity to terminate during whole-cell Ca^{2+} responses. They further buttress other evidence that the decline in SD signal during the rising phase of the response does not arise because the indicator dye becomes saturated, but faithfully reflects a physiological termination of puff activity.

Partial depletion of ER Ca^{2+} selectively inhibits Ca^{2+} puffs.

We next considered the possibility that puff activity may terminate during the rising phase of global Ca^{2+} elevations because of falling luminal ER [Ca^{2+}], rather than rising cytosolic [Ca^{2+}]. We tested this idea by imaging i-IP_3 evoked global Ca^{2+} signals after partially depleting ER Ca^{2+} stores while minimizing changes in cytosolic free [Ca^{2+}].

In a first approach (Fig. 5A) we transiently applied cyclopiazonic acid (CPA) to reversibly inhibit SERCA activity[41], resulting in a net leak of Ca^{2+} from the ER and a small elevation of cytosolic Ca^{2+}. Following wash-out of CPA, the cell was maintained in Ca^{2+}-free medium so that the cellular Ca^{2+} content (including that of the ER) gradually depleted owing to passive and active extrusion across the plasma membrane. After about 4 min the resting cytosolic Ca^{2+} level had returned close to

449 the original baseline, and we delivered a photolysis flash to photorelease i-IP_3. This
450 evoked a substantial elevation in global Ca^{2+}, yet the SD signal showed almost no
451 transient puff activity during this response. Similar results were obtained in a
452 further 7 cells, as shown by the mean $\Delta F/F_0$ and SD traces in Fig. 5B. To confirm
453 that the suppression of puff activity resulted from cellular Ca^{2+} depletion, we
454 repeated this experiment, now making a paired comparison of i-IP_3-evoked
455 responses between cells that were bathed for 30 min after washing out CPA either
456 in Ca^{2+}-containing medium to allow ER store refilling (Fig. 5C), or in Ca^{2+}-free
457 medium (Fig. 5D). Cells in both groups showed substantial global Ca^{2+} responses
458 that were not appreciably different in peak amplitudes (Fig. 5E); but whereas the
459 SD signals showed that puff activity was strongly suppressed in cells maintained in
460 zero Ca^{2+} medium, cells in Ca^{2+}-containing medium showed robust puff activity
461 during the rising phase of the response (Fig. 5F; supplemental movie M5).
462
463 As an alternative approach to partially deplete ER Ca^{2+} without pharmacological
464 intervention, we evoked Ca^{2+} signals by repeated applications of CCH at 5 min
465 intervals, and compared responses in cells bathed in Ca^{2+}-containing (Fig. 5G) and
466 Ca^{2+}-free solutions (Fig. 5H). In both cases the amplitudes of the global Ca^{2+} signals
467 progressively declined, likely a result of inhibition of IP_3Rs. However, whereas the
468 amplitude of puff activity reported by SD signals in cells bathed in Ca^{2+}-containing
469 medium fell roughly in proportion to the amplitude of the global fluorescence signal,
470 puff activity in Ca^{2+}-free medium declined abruptly. In the example depicted in Fig.
471 5H, no activity was evident in the SD signal after the fifth stimulus at 20 min even

472 though an appreciable global Ca^{2+} elevation remained. To quantify these data, we
473 determined puff activity as the integral under the SD trace, and plotted the
474 normalized ratio of puff activity vs. peak global Ca^{2+} amplitude (Fig. 5I). For cells in
475 Ca^{2+}-containing medium the mean ratio remained constant across successive stimuli
476 (blue squares, Fig. 5I), whereas it declined almost to zero for cells in Ca^{2+}-free
477 medium (red circles, Fig. 5I).
478
479 We conclude from these results that Ca^{2+} puff activity is modulated by ER Ca^{2+} store
480 content, and that when stores are partially depleted IP_3 can still evoke Ca^{2+} release
481 by a process that is independent of puff activity, and occurs without detectable
482 temporal fluctuations. We term this mode of Ca^{2+} liberation as 'diffuse' release, and
483 refer to Ca^{2+} puffs as a 'punctate' mode of Ca^{2+} liberation.
484
485 **All three IP_3R isoforms mediate punctate and diffuse modes of Ca^{2+} liberation.**
486 In common with many other cell types, WT HEK and HeLa cells express all three
487 major IP_3R isoforms – types 1, 2, and 3 – that are encoded by separate genes and
488 translated into structurally and functionally distinct proteins that co-translationally
489 oligomerize to form heterotetrameric channels. We[42] and others[25] recently
490 demonstrated that all three isoforms can individually mediate Ca^{2+} puffs. We now
491 utilized HEK cells genetically engineered to express single IP_3R isoforms to evaluate
492 the respective roles of each isoform in liberating Ca^{2+} via punctate, localized
493 transients versus sustained, diffuse release.
494

We evoked Ca^{2+} liberation in WT HEK cells and cells exclusively expressing type 1, 2, or 3 IP_3Rs by local application of CCH (Fig. 6). All three single-isoform-expressing cell lines exhibited patterns of responses qualitatively similar to WT cells. The SD traces showed flurries of puffs during the foot and rising phase of global Ca^{2+} signals that ceased before the time of the peak global Ca^{2+} elevation (Fig. 6A-H**).** Nevertheless, notable differences were apparent between the isoforms. Cells expressing IP_3R1 generated whole-cell Ca^{2+} signals having much smaller amplitudes and slower rising phases than WT and R2- and R3-expressing cells, and localized fluctuations persisted longer (Fig. 6C,D,I). In contrast, IP_3R2-expressing cells displayed fast rising, large amplitude Ca^{2+} signals, with a transient flurry of Ca^{2+} fluctuations concentrated during the initial portion of the rising phase (Fig. 6E,F). Ca^{2+} signals in cells expressing IP_3R3 (Fig. 6G,H) were similar in amplitude to WT and IP_3R2-expressing cells, but with slower rates of rise and more prolonged flurries of puffs. Scatter plots of puff activity (SD signal) as a function of the global Ca^{2+} level ($\Delta F/F_0$) during the rising phase of the global response further highlighted these differences (Fig. 6J,K). Ca^{2+} fluctuations were maximal when Cal520 fluorescence ($\Delta F/F_0$) rose to roughly 1.5, 6, and 3 for type 1, 2, and 3 IP_3Rs, respectively; and similarly large differences were evident in the global Ca^{2+} level attained when puff activity terminated.

Diffuse Ca^{2+} signals in TIRF do not reflect punctate release in the cell interior

The data in Figs 1-6 derive from TIRF imaging of Ca^{2+} signals in close proximity to the plasma membrane, where a majority (~80%) of puff sites in WT HEK cells are

located[42]. However, TIRF microscopy provides no direct information from the interior of the cell, leaving open the question as to whether slow diffusion of Ca^{2+} ions from puffs at internal sites may contribute to the diffuse component of the Ca^{2+} signal visualized in TIRF images after the puff flurry has ceased. To address this issue, we applied fluctuation analysis to images obtained using lattice light-sheet (LLS) microscopy to record Ca^{2+} signals within diagonal optical 'slices' through the cell volume[43].

Fig. 7A,B illustrate LLS Ca^{2+} fluorescence ratio images and corresponding SD images recorded before and after photorelease of i-IP_3 to evoke a global Ca^{2+} response. Similar to observations with TIRF imaging, the SD images revealed local Ca^{2+} transients that began soon after photorelease, and before any appreciable rise in the global Ca^{2+} signal (Fig. 7A, panel ii). Discrete events then continued during much of the rising phase of the global signal (panels iii-v) but had largely ceased at the time of the peak global signal (panel vi). In this cell Ca^{2+} puffs were primarily restricted to the cell periphery, whereas Fig. 7B shows an example from another cell where local activity was observed both around the periphery and in the cell interior.

Figs. 7C,D shows respective measurements from these two cells, plotting fluorescence ratio changes ($\Delta F/F_0$) and SD signals from ROIs encompassing peripheral (red traces) and central (blue traces) regions of the cells, as indicated in the leftmost lower panels of Figs. 7A,B. In both cells, the local Ca^{2+} activity monitored by SD fluctuations started within a few hundred ms of the photolysis

flash and was maximal during the early portion of the rising phase. The SD signal then declined, returning close to baseline as the global Ca^{2+} signal approached a peak. For the cell illustrated in Fig. 7A, the SD signal within the peripheral region was much greater than in the central region, even though the rise in global Ca^{2+} was slightly smaller. In contrast, the cell illustrated in Fig. 7B showed a SD signal in the interior that was similar in size to the periphery (Fig. 7D). On average, however, mean SD signals from the cell interior were about one quarter of that at the periphery, and fluctuations arising from interior sites followed a similar relation with bulk Ca^{2+} level as peripheral sites (Fig. 7E).

Given the relatively low average level of puff activity in the cell interior, and the similar termination of internal and peripheral puff flurries during the rising of global Ca^{2+} signals, we conclude that the diffuse component of the Ca^{2+} rise observed by TIRF microscopy cannot be accounted for by Ca^{2+} spreading from punctate release at internal sites and becoming blurred by diffusion in space and time.

Puff activity contributes only a fraction of the total Ca^{2+} liberated during global signals.

To assess the relative contributions of punctate versus diffuse modes of Ca^{2+} release during global Ca^{2+} signals, we derived the kinetics of Ca^{2+} flux into the cytosol through IP_3Rs on the basis that the cell-wide fluorescence signal reflects a balance between Ca^{2+} release into the cytoplasm and its subsequent removal. To obtain a rate constant for removal of cytosolic Ca^{2+} in WT HEK cells, we recorded the decline

564 of fluorescence Ca^{2+} signals following transient photorelease of Ca^{2+} from caged
565 Ca^{2+} loaded into the cytosol (Supplemental fig. S9A), and during the final 'tail' of
566 CCH-evoked Ca^{2+} signals when Ca^{2+} liberation would have almost ceased
567 (Supplemental fig. S9B). Both fitted well to single exponential decay functions,
568 consistent with a dominantly first order removal process, with respective mean rate
569 constants of 0.22 and 0.32 s^{-1}.
570
571 We then calculated the instantaneous Ca^{2+} release flux at intervals throughout the
572 time course of a global Ca^{2+} response by differentiating the whole-cell fluorescence
573 Ca^{2+} signal and adding to this the estimated rate of Ca^{2+} removal; for i-IP_3 signals we
574 used a rate constant of 0.22 s^{-1}; for CCH evoked responses we applied rate constants
575 (0.3 s^{-1} to 0.6 s^{-1}) that were determined from the tail-end of the global Ca^{2+} decay for
576 that particular cell.
577
578 We used data from the experiment of Fig. 5C,D to compare the kinetics of Ca^{2+}
579 liberation during Ca^{2+} signals under normal conditions, and when puff activity had
580 been inhibited by partial depletion of ER Ca^{2+} store content. Figs. 8A,B show records
581 from two representative cells that gave global Ca^{2+} responses of comparable peak
582 amplitudes (black traces). However, whereas the SD signals (grey traces) exhibited
583 the normal flurry of puff activity in the control cell (Fig. 8A) this activity was almost
584 completely suppressed in the cell pretreated with CPA (Fig. 8B). The red traces
585 show the respective rates of Ca^{2+} release into the cytosol, revealing a larger initial
586 transient of Ca^{2+} liberation in the control cell during the flurry of puff activity. Fig.

587 8C shows overlaid mean traces of Ca^{2+} release from control (n = 5) and CPA-treated
588 cells (n = 6). Colored areas indicate the relative cumulative amounts of Ca^{2+}
589 entering the cytosol (integral under the release trace) in CPA-treated cells where
590 puff activity was substantially abolished (blue shading), and the additional Ca^{2+} flux
591 (pink shading) in control cells showing flurries of puffs. From these respective
592 areas we estimate that, in normal conditions, the punctate liberation of Ca^{2+} through
593 puff activity contributes about 41% of the total Ca^{2+} release responsible for the
594 initial rise of Ca^{2+} toward its peak. Figs. 8D,E further illustrate representative
595 records of SD signals (grey traces), global Ca^{2+} (black), rate of Ca^{2+} release into the
596 cytosol (red), and cumulative amount of Ca^{2+} released (blue) during the entire time
597 course of global Ca^{2+} signals evoked by photoreleased i-IP_3 (Fig. 8D) and by CCH
598 (Fig. 8E). Because much of the cumulative Ca^{2+} release through IP_3Rs arises from a
599 sustained, low level flux that continues after the peak, Ca^{2+} puffs on average
600 contribute only about 13% of the total Ca^{2+} liberation during global i-IP_3-evoked
601 signals, and about 17% during shorter-lasting responses evoked by CCH (Fig. 8F).
602
603
604 **DISCUSSION**
605 Ca^{2+} puffs are transient, localized elevations in cytosolic Ca^{2+} that arise from
606 concerted opening of small numbers of IP_3Rs clustered at fixed intracellular sites[3,44].
607 Puffs are apparent as discrete events superimposed on a steady basal Ca^{2+} level
608 when cytosolic IP_3 concentrations are modestly elevated[3,4,9], whereas higher
609 concentrations of IP_3 evoke global, cell-wide Ca^{2+} signals on which puffs are evident

610 on the rising phase[8,18]. Puffs have been proposed as fundamental building blocks of
611 IP_3-mediated Ca^{2+} signaling[8,9,13,14,17,18,25]; acting as local signals in their own right at
612 low [IP_3] and mediating global Ca^{2+} signals at higher [IP_3] by a fire-diffuse-fire
613 mechanism whereby Ca^{2+} released by a puff site diffuses to activate CICR at
614 neighboring sites[8,9,13,16]. However, it has been difficult to definitively test this
615 'building block' model because puffs become obscured by the large global Ca^{2+}
616 elevations; and recent theoretical simulations have questioned whether the
617 summation of Ca^{2+} released through coordinated puff activity at multiple sites is
618 alone sufficient to propagate global cytosolic Ca^{2+} signals[24]. Here, we addressed this
619 topic by analyzing temporal and spatial fluctuations in Ca^{2+} image data to resolve
620 local Ca^{2+} transients during global signals[29]. Our main conclusion is that global Ca^{2+}
621 signals involve two modes of Ca^{2+} liberation through IP_3Rs: 'punctate' release as a
622 flurry of transient, local events, and a more sustained, 'diffuse' release mode.
623
624 As with any new approach, we first needed to validate the ability of our algorithm to
625 faithfully report local Ca^{2+} transients during even large global Ca^{2+} elevations, when
626 resolution may be impaired by factors including the dynamic range of the indicator
627 dye and by increased photon shot noise at high fluorescence levels. A particular
628 concern was whether the indicator (Cal520) we used for most experiments may
629 have approached saturation, thus 'clipping' the signals to artifactually suppress the
630 temporal SD signal and giving a false impression that puff activity terminates as the
631 Ca^{2+} level and fluorescence rise during global signals. Several lines of evidence
632 convincingly argue that this is not the case. Notably: (i) maximal, saturating signals

633 evoked by ionomycin (~19 $\Delta F/F_0$) were much higher than mean peak IP_3-evoked
634 fluorescence signals (~7 $\Delta F/F_0$), and puff activity began to decline as fluorescence
635 rose above ~2 $\Delta F/F_0$; (ii) we observed patterns of puff activity using the low affinity
636 indicator fluo-8L (K_d 1.86 μM) that closely matched those obtained with Cal520 (K_d
637 320 nM) (Supplemental fig. S5); (iii) we were able to resolve instances of local puff
638 activity even at the peak of IP_3-evoked global fluorescence elevations (Supplemental
639 fig. S4); (iv) the kinetics of puff activity were closely similar in cell lines individually
640 expressing single IP_3R isoforms, despite large differences in the amplitudes of the
641 global Ca^{2+} signals (Fig. 6); (v) the onset and termination of puff activity during the
642 rise of IP_3-mediated global Ca^{2+} signals were little altered when the initial basal Ca^{2+}
643 level was elevated (Fig. 4A,B) or, conversely, when the global Ca^{2+} rise was
644 attenuated by buffering with cytosolic EGTA (Fig. 4C,D). Finally, the suppression of
645 punctate Ca^{2+} liberation throughout all phases of IP_3-evoked Ca^{2+} responses when
646 ER Ca^{2+} stores were partially depleted (Fig. 5) strongly supports our proposal that
647 Ca^{2+} liberation can arise in a diffuse manner, independent of local puff events.
648
649 *Puff activity during global Ca^{2+} signals*
650 In agreement with previous findings[8,18] our fluctuation analyses reveal flurries of
651 puffs during the initial rise of IP_3-mediated global Ca^{2+} signals. However, although
652 puff activity was evident during the initial foot of the response and peaked early
653 during the rising phase, it then subsided during the later portion of the rising phase,
654 with few or no transient, local Ca^{2+} signals evident by the time of the peak. Notably,
655 overall Ca^{2+} levels continued to rise after puffs had largely ceased, and cytosolic Ca^{2+}

656 remained elevated for several seconds in the face of rapid removal from the cytosol,
657 during which time Ca^{2+} fluctuations were largely suppressed.
658
659 This 'noise-free' component of the fluorescence signal cannot be attributed to slow
660 diffusion of Ca^{2+} liberated as puffs to fill in spaces between release sites. Diffusion
661 would be rapid (e.g. mean time of ~300 ms to diffuse 5 μm assuming an effective
662 diffusion coefficient of 20 $\mu m^2\ s^{-1}$*).* In any case, the average fluorescence signal
663 would not be expected to increase appreciably if the total amount of Ca^{2+} in the
664 imaging volume remained constant. Utilizing lightsheet imaging we further excluded
665 the possibility that the continuing rise in near-plasmalemmal Ca^{2+} observed by TIRF
666 imaging might arise through diffusion of Ca^{2+} over longer distances after liberation
667 at sites in the cell interior. Finally, as noted previously, the observation of large
668 global Ca^{2+} signals in the absence of detectable fluorescence fluctuations (Fig. 5)
669 definitively points to a mode of Ca^{2+} liberation that is independent of puff activity.
670
671 By deriving the time course of cumulative Ca^{2+} liberation during global responses
672 we estimated that puffs contribute only ~41% of the initial Ca^{2+} flux that drives the
673 peak of the Ca^{2+} response, and an even smaller proportion (~15%) of the
674 cumulative flux during its entire time course. Thus, a second component of
675 continuous, spatially diffuse release of intercellular Ca^{2+} is responsible for
676 generating and sustaining a large part of whole-cell Ca^{2+} signals. These two
677 components are further discriminated by procedures that selectively promoted
678 either puff activity[27,28] (by cytosolic loading of slow Ca^{2+} buffers), or global Ca^{2+}

679 elevations in the absence of localized Ca^{2+} transients (by partial depletion of ER Ca^{2+}
680 store content). We term these two modes of IP_3-mediated Ca^{2+} release as 'punctate'
681 (discontinuous in time and space) and 'diffuse' (smoothly varying in time and
682 space).
683
684 Small elevations of [Ca^{2+}] promote opening of IP_3R channels[11,12] and increase puff
685 frequency[45]. The accelerated puff activity during the foot and initial upstroke of the
686 global Ca^{2+} signal is thus likely a consequence of a rising basal cytosolic Ca^{2+} level,
687 resulting both from the puffs themselves and from diffuse Ca^{2+} liberation. This
688 positive feedback of cytosolic Ca^{2+} to promote opening of IP_3Rs is inherently
689 regenerative, so it is imperative that mechanisms exist to 'put out the fire'. Our
690 results illuminate at least two mechanisms, acting across different time scales, to
691 terminate punctate Ca^{2+} liberation through IP_3Rs. Individual puffs terminate rapidly
692 as IP_3R channels close within tens of ms[9,46] via stochastic inhibition by high local
693 Ca^{2+} levels[47] and potential allosteric interactions between clustered IP_3Rs at a puff
694 site[48]. However, during the rising phase of a global Ca^{2+} signal, each IP_3R cluster may
695 generate a flurry of repeated puffs - indicating that although the fast-inhibitory
696 processes that terminates individual puffs recovers quickly, a slower process
697 terminates the flurry. This does not appear to result from IP_3Rs becoming
698 inactivated by the rise of bulk cytosolic Ca^{2+}, because we found puff flurries were
699 not suppressed by prior Ca^{2+} elevations, and still terminated normally during global
700 responses when cytosolic Ca^{2+} levels were attenuated by buffering with EGTA (Fig.
701 4C,D). Instead, our observations that partial depletion of ER Ca^{2+} stores suppressed

puff activity during global Ca^{2+} responses (Fig. 5) implicate the depletion of luminal Ca^{2+} as a dominant mechanism responsible for terminating the local signals; analogous to the central role of luminal Ca^{2+} depletion in terminating the Ca^{2+} sparks mediated by ryanodine receptors[49]. Although individual puffs appear not to affect luminal ER $[Ca^{2+}]$[42], it is plausible that ER depletion may occur during the rapid flurries of puffs evoked at multiple sites during the rising phase of global signals. A related question is whether the Ca^{2+} depletion is locally confined to the ER around puff sites and arises through Ca^{2+} released by the puffs themselves, or whether diffuse Ca^{2+} liberation causes global ER Ca^{2+} depletion throughout a luminally continuous ER network[50,51].

Two functionally distinct modes of IP_3R-mediated Ca^{2+} liberation

The two modes of Ca^{2+} liberation we describe – punctate and diffuse – might, in principle, arise from two functionally and physically distinct populations of IP_3Rs, or through functional regulation of the clustered IP_3Rs underlying puffs such that they switch from a pulsatile to continuous mode of release. At present we cannot discriminate between these mechanisms, but favor the former for congruence with studies revealing two distinct populations of IP_3Rs in terms of their spatial distributions and motilities. A small (~30%) fraction of the IP_3Rs in a cell are stationary[44,52], grouped in small clusters that are anchored at fixed sites predominantly near the plasma membrane[28,42,44], whereas the majority of IP_3Rs are distributed throughout the bulk of the cytoplasm and are motile within the ER membrane[44,52–56]. Puffs are proposed to originate from IP_3Rs within the immotile

clusters that are endowed with the ability to preferentially respond to low concentrations of IP_3[28,44]. In contrast, the widely distributed, motile IP_3Rs remain apparently silent under conditions when puffs are selectively activated by low concentrations of IP_3 or in the presence of slow cytosolic Ca^{2+} buffers to inhibit global Ca^{2+} elevations[27,57]. The motile, distributed IP_3Rs would be an attractive candidate for the diffusive mode of Ca^{2+} liberation.

Functional differences between putative populations of IP_3Rs mediating punctate and diffuse Ca^{2+} release cannot be attributed to their being constituted of different isoforms of IP_3R, because all three isoforms mediate Ca^{2+} puffs[25,42], and we show here that cells exclusively expressing individual isoforms generate cell-wide Ca^{2+} elevations involving both punctate and diffuse modes of Ca^{2+} liberation. Instead, the functional properties of the IP_3Rs may be affected by factors including their location in the cell, their mutual proximity to enable interactions by CICR, and by their association with modulatory and anchoring proteins[58–60].

Consequences of bimodal Ca^{2+} signals for downstream signaling

Stimulation of the IP_3/Ca^{2+} signaling pathway by activation of cell-surface receptors evokes repetitive oscillations in cytosolic Ca^{2+} in numerous cell types[61]. Signaling information is encoded in the amplitude and frequency of these Ca^{2+} oscillations, which may have periods ranging widely from a few seconds to minutes. Classical studies illustrate how different frequencies of Ca^{2+} oscillations activate distinct targets, including the selective activation of NFkB in Jurkat T cells by low

748 frequencies[62], and the frequency-dependent control of gene expression in RBL mast
749 cells[63]. However, signaling information is not restricted to frequency and amplitude
750 components of bulk cytosolic Ca^{2+} elevations, and numerous findings implicate a
751 component of spatial Ca^{2+} profiling[7,64–66]. Because of the restricted diffusion of free
752 Ca^{2+} ions in the cytosol[67,68], the specificity of downstream signaling by Ca^{2+} liberated
753 through IP_3Rs will be strongly influenced by the proximity of target proteins, as well
754 as by their Ca^{2+} binding kinetics[69–71]. The two modes of IP_3-evoked Ca^{2+} liberation
755 we describe are, therefore, likely to selectively activate different populations of
756 effectors; those positioned close to the IP_3Rs at puff sites that experience brief,
757 repetitive transients of high local [Ca^{2+}], and others that respond to a more
758 sustained, spatially diffuse elevation of bulk cytosolic [Ca^{2+}].
759
760 Based on a close juxtaposition of stationary IP_3R clusters to ER-plasma membrane
761 junctions where STIM and Orai interact to induce store-operated Ca^{2+} entry
762 (SOCE)[44,72] it has been proposed that local depletion of ER Ca^{2+} content at puff sites
763 might rapidly and selectively activate SOCE, without requiring substantial overall
764 loss of the ER Ca^{2+} that is necessary to sustain numerous ER functions[44,72,73]. On the
765 other hand, we previously reported puffs to be unaffected by removal of
766 extracellular Ca^{2+}[42], and we show that patterning of local puff activity during IP_3-
767 evoked global Ca^{2+} signals is unaffected by the presence or absence of Ca^{2+} in the
768 bath solution. Thus, influx of extracellular Ca^{2+} does not appear to contribute acutely
769 to the initial flurry of puffs or to the rapid rise in global Ca^{2+}, although the more
770 prolonged decay phase of the Ca^{2+} signal in Ca^{2+}-containing medium points to a

771 slower activation of SOCE. The relative contributions of local puffs vs. diffuse Ca^{2+}
772 liberation in activating SOCE remain to be determined. Another example of
773 proximate Ca^{2+} signaling is the close tethering between ER and mitochondria[74] that
774 underlies a rapid shuttling of Ca^{2+} released through IP_3Rs to the mitochondrial
775 matrix[71,75], such that Ca^{2+} transients within a signaling microdomain, rather than the
776 bulk cytosolic Ca^{2+} signal, regulate mitochondrial bioenergetics and induction of
777 autophagy[76]. A similar close coupling has recently been described between IP_3Rs
778 and lysosomes[70]. Our description of two modes of IP_3-mediated Ca^{2+} liberation thus
779 raises questions regarding their respective roles in downstream signaling. Is
780 organellar Ca^{2+} signaling via structurally defined nanodomains restricted to the
781 predominantly peripheral ER contact sites where puffs originate, or might a
782 separate population of IP_3Rs that mediate diffuse Ca^{2+} liberation also transmit their
783 signals via restricted domains?
784
785
786 **METHODS**
787 *Cell Culture and loading*
788 HEK293 wild-type (WT) cells were kindly provided by Dr. David Yule (University of
789 Rochester). An IP_3R null cell line (3KO; #EUR030) and cell lines natively expressing
790 exclusively type 1 (IP_3R1; #EUR031), type 2 (IP_3R2; #EUR032) and type 3 (IP_3R3;
791 #EUR033) isoforms generated from that parental WT HEK293 cell line by
792 CRISPR/Cas9 genetic engineering in the Yule lab were purchased from Kerafast
793 (Boston, MA). HeLa cells (#CCL-2) were purchased from ATCC (Manassas, VA). HEK

794 WT, 3KO, and single IP_3R isoform-expressing cell lines were cultured in Eagle's
795 Minimum Essential Medium (EMEM; ATCC #30-2003), and HeLa cells were cultured
796 in Dulbecco's modified Eagle Medium (DMEM; #11965092) from Thermo Fisher
797 Scientific (Waltham, MA). Both EMEM and DMEM were supplemented with 10%
798 fetal bovine serum (#FB-11) from Omega Scientific (Tarzana, CA). All cell lines were
799 cultured in plastic 75 cm flasks and maintained at 37^{o}C in a humidified incubator
800 gassed with 95% air and 5% CO_2. For imaging, cells were collected using 0.25%
801 Trypsin-EDTA (Thermo Fisher Scientific #25200-056) and grown on poly-D-lysine
802 (Millipore Sigma #P0899; St. Louis, MO) coated (1 mg/ml) 35-mm glass bottom
803 imaging dishes (#P35-1.5-14-C) from MatTek (Ashland, MA) or 12 mm glass
804 coverslips for 2-3 days.
805
806 Immediately before imaging, cells were incubated with the membrane-permeant
807 fluorescent Ca^{2+} indicator Cal520/AM (5 μM; AAT Bioquest #21130; Sunnyvale, CA)
808 for 1 hr at room temperature (RT) in a Ca^{2+}-containing HEPES buffered salt solution
809 (Ca^{2+}-HBSS). Where indicated cells were additionally loaded with membrane
810 permeant esters of either the caged IP_3 analogue ci-IP_3/PM [D-2,3,-O-
811 Isopropylidene-6-O-(2-nitro-4,5 dimethoxy) benzyl-myo-Inositol 1,4,5,-
812 trisphosphate Hexakis (propionoxymethyl) ester] (1 μM; SiChem #cag-iso-2-145-
813 10; Bremen, Germany) or the caged Ca^{2+} buffer NP-EGTA [o-nitrophenyl EGTA/AM]
814 (200 - 500 nM; Thermo Fisher Scientific #N6803) in conjunction with Cal520. For
815 the experiments in Fig. 4C,D cells were additionally loaded with EGTA/AM (15 μM;
816 Thermo Fisher Scientific #E1219) for 1 hr at RT in Ca^{2+}-HBSS to attenuate global

817 Ca^{2+} elevations. To address possible saturation of Cal520 at high Ca^{2+} levels, cells
818 were alternatively loaded with the lower affinity Ca^{2+} indicator fluo8L/AM (5 μM,
819 AAT Bioquest #21096) together with 1 μM ci-IP_3/PM for 1 hr at RT in Ca^{2+}-HBSS.
820 Following incubation with AM esters, cells were incubated for 30 min at room
821 temperature in Ca^{2+}-HBSS. Cal520/AM, ci-IP_3/PM, and NP-EGTA/AM, EGTA/AM, and
822 fluo8L/AM were all solubilized with DMSO/20% pluronic F127 (Thermo Fisher
823 Scientific #P3000MP).
824
825 FCCP (carbonyl cyanide p-(trifluoromethoxy) phenylhydrazone) and CPA
826 (cyclopiazonic acid), were purchased from Millipore Sigma (#C2920 and #C1530,
827 respectively), and solubilized in 100% ethanol. Carbachol (#C4832) and histamine
828 (#H7125), also from Millipore Sigma, were reconstituted in deionized H_2O. Ca^{2+}-
829 HBSS contained (in mM) 135 NaCl, 5.4 KCl, 2 $CaCl_2$, 1 $MgCl_2$, 10 HEPES, and 10
830 glucose (pH=7.4). Nominal Ca^{2+}-free HBSS consisted of the same formulation as
831 Ca^{2+}-HBSS except that $CaCl_2$ was omitted; for zero Ca^{2+}-HBSS, 300 μM EGTA was
832 added to nominal Ca^{2+}-free HBSS. For lattice light-sheet imaging, the plasma
833 membrane was stained by adding Cell Mask Deep Red (Thermo Fisher Scientific
834 #C10046) to the bathing solution in the imaging chamber at 1/50,000 dilution.
835
836 *Ca^{2+} imaging*
837 Total internal reflection fluorescence (TIRF) imaging of Ca^{2+} signals was
838 accomplished using a home-built system, based around an Olympus (Center Valley,
839 PA) IX50 microscope equipped with an Olympus 60X oil immersion TIRF objective

840 (NA 1.45). Fluorescence images were acquired with an Evolve EMCCD camera
841 (Photometrics; Tucson, AZ) with a bit depth of 16 bits, using 2x2 binning for a final
842 field at the specimen of 128 × 128 binned pixels (1 binned pixel = 0.53μm) at a rate
843 of ~ 125 frames s^{-1}. Image data were streamed to computer memory using
844 Metamorph v7.7 (Molecular Devices; San Jose, CA) and stored on hard disk for
845 offline analysis.
846
847 Lattice light-sheet imaging was performed using a home-built system as previously
848 described[43]. Images were acquired with an Andor Zyla 4.2 sCMOS camera (Oxford
849 Instruments; Abingdon, England) from a single, diagonal light-sheet slice (512 x 256
850 pixels, 1 pixel = 0.11 μm) at 100 frames s^{-1} and 16 bit depth. Ca^{2+} signals were
851 imaged in Cal520-loaded cells for several seconds following photorelease of i-IP_3 by
852 a flash from a 405 nm laser diode, utilizing 473 nm laser fluorescence excitation and
853 a 510-560 nm bandpass emission filter. A 562 nm laser and 590 nm long-pass filter
854 were used to image the plasma membrane stained with Cell Mask Deep Red. Images
855 were streamed to disk using MicroManager (Vale Lab UCSF; San Francisco, CA).
856
857 *Photo-uncaging and local application of agonist*
858 Photorelease of i-IP_3 was evoked by UV light from a xenon arc lamp filtered through
859 a 350–400 nm bandpass filter and introduced by a UV-reflecting dichroic in the light
860 path to uniformly illuminate the field of view. The amount of i-IP_3 released was
861 controlled by varying the flash duration, set by an electronically controlled shutter
862 (UniBlitz; Rochester, NY). The same system was used for photolysis of NP-EGTA (i.e.

863 caged Ca^{2+}). For the local delivery of solutions to cells during imaging, glass
864 micropipettes were prepared from borosilicate glass capillary filaments (1.5mm x
865 0.86mm, O.D. x I.D.) using a micropipette puller (Sutter Instruments; Novato, CA) to
866 produce tip diameters of ~1-2 µm. Micropipettes were positioned above the cell
867 understudy with local delivery controlled using a pneumatic picospritzer. The
868 delivery of micropipette contents and the duration and intensity of the UV-flash
869 were empirically adjusted to evoke rapid rises in whole-cell cytosolic Ca^{2+} levels.
870
871 All imaging was performed while cells were bathed in HBSS containing 2 mM Ca^{2+} or
872 zero Ca^{2+}-HBSS containing 0.3 mM EGTA and no added Ca^{2+}.
873
874 *Image Analysis*
875 Image data imported in16 bit integer MetaMorph stk or multi-plane TIF format
876 were processed using a script written in Flika (http://flika-org.github.io), a freely
877 available open-source image processing and analysis software in the Python
878 programming language[26,77]. All internal processing and data output were
879 performed using 64 bit floating-point arithmetic.
880
881 To analyze and derive movies representing the pixel-by-pixel standard deviation
882 (SD) of *temporal* fluctuations in fluorescence of the Ca^{2+} indicator dye we used a
883 custom Flika script as described previously[26]. In brief, following subtraction of
884 camera black offset level, the raw image stack from the camera was first spatially
885 filtered by a Gaussian blur function with a standard deviation (sigma) of 2 pixels

886 (~1 μm at the specimen). The python package (skimage) used to perform this
887 function applies a two-dimensional Gaussian blur with a specified standard
888 deviation (sigma) out to a range of 4 sigma. To attenuate high frequency photon
889 shot noise and slow changes in baseline fluorescence, it was then temporally filtered
890 with a bandpass Butterworth filter with low and high cutoff frequencies of 3 and 20
891 Hz. A running variance of this temporally filtered movie was calculated, pixel by
892 pixel, by subtracting the square of the mean from the mean of the square of a
893 moving 20 frame (160 ms) boxcar window of the movie. The running standard
894 deviation was calculated by taking the square root of the variance image stack to
895 create a standard deviation (SD) stack. Finally, to remove the mean predicted
896 photon shot noise which increases in linear proportion to the mean fluorescence
897 intensity, the SD stack was corrected, pixel-by-pixel, by subtracting the square root
898 of a running mean of the spatially filtered fluorescence movie multiplied by a scalar
899 constant; derived as illustrated in Supplemental fig. S2.
900
901 We also applied a second FLIKA script to analyze *spatial* fluctuations in Ca^{2+} image
902 stacks. For this, black-level subtracted image stacks were first temporally band-pass
903 filtered as before, and then new image stacks were derived by taking the difference
904 of weak (sigma 2 pixel) and stronger (sigma 8 pixel) Gaussian blur functions.
905 Essentially, this functioned as a spatial bandpass filter, attenuating high frequencies
906 caused by pixel-to-pixel shot noise variations and low frequency variations resulting
907 from spread of Ca^{2+} waves across the cell, while retaining spatial frequencies
908 corresponding to the spread of local Ca^{2+} puffs. Next, for each frame we calculated

the spatial variance among pixels within an imaging field, took the square root to obtain a measure of the spatial SD signal and subtracted the predicted increase in spatial shot noise with increasing fluorescence. Finally, we derived traces showing the average spatial fluctuations across a region encompassing the entire cell within a moving boxcar window of 160 ms (Supplemental fig. S3).

The scripts used to perform temporal and spatial fluctuation analysis are presented as Supplemental Material.

Acknowledgements

We thank Dr. Carley A. Karsten for assisting in initial imaging experiments and Dr. Kyle L. Ellefsen for help with software and image analysis.

Funding Sources

This work was supported by NIH grant R37 GM048071 (I.P.)

Author contributions

IP directed the project and conceived the fluctuation analysis technique. IP and JTL performed experiments, analyzed data and wrote the manuscript.

Competing interests

The authors declare no competing interests.

BIBLIOGRAGPHY

1. Clapham, D. E. Calcium Signaling. *Cell* **131**, 1047–1058 (2007).
2. Berridge, M. J., Lipp, P. & Bootman, M. D. The versatility and universality of calcium signalling. *Nat Rev Mol Cell Biol* **1**, 11–21 (2000).
3. Parker, I. & Yao, Y. Regenerative release of calcium from functionally discrete subcellular stores by inositol trisphosphate. *Proc. R. Soc. B Biol. Sci.* **246**, 269–274 (1991).
4. Yao, Y., Choi, J. & Parker, I. Quantal puffs of intracellular Ca2+ evoked by inositol trisphosphate in Xenopus oocytes. *J. Physiol.* **482**, 533–553 (1995).
5. Woods, N. M., Cuthbertson, K. S. R. & Cobbold, P. H. Repetitive transient rises in cytoplasmic free calcium in hormone-stimulated hepatocytes. *Nature* **319**, 600–602 (1986).
6. Parekh, A. B. Decoding cytosolic Ca2+ oscillations. *Trends Biochem. Sci.* **36**, 78–87 (2011).
7. Smedler, E. & Uhlén, P. Frequency decoding of calcium oscillations. *Biochim. Biophys. Acta - Gen. Subj.* **1840**, 964–969 (2014).
8. Bootman, M. D., Berridge, M. J. & Lipp, P. Cooking with Calcium: The Recipes for Composing Global Signals from Elementary Events. *Cell* **91**, 367–373 (1997).
9. Parker, I., Choi, J. & Yao, Y. Elementary events of InsP3-induced Ca2+ liberation in Xenopus oocytes: hot spots, puffs and blips. *Cell Calcium* **20**, 105–121 (1996).
10. Parker, I. & Ivorra, I. Inhibition by Ca2+ of inositol trisphosphate-mediated

Ca2+ liberation: a possible mechanism for oscillatory release of Ca2+. *Proc. Natl. Acad. Sci.* **87**, 260 LP – 264 (1990).

11. Iino, M. Biphasic Ca2+ dependence of inositol 1,4,5-trisphosphate-induced Ca release in smooth muscle cells of the guinea pig taenia caeci. *J. Gen. Physiol.* **95**, 1103–22 (1990).

12. Bezprozvanny, llya, Watras, J. & Ehrlich, B. E. Bell-shaped calcium-response curves of lns(l,4,5)P3- and calcium-gated channels from endoplasmic reticulum of cerebellum. *Nature* **351**, 751–754 (1991).

13. Berridge, M. J. Elementary and global aspects of calcium signalling. *J. Physiol.* **499**, 291–306 (1997).

14. Bootman, M. D. & Berridge, M. J. Subcellular Ca2+ signals underlying waves and graded responses in HeLa cells. *Curr. Biol.* **6**, 855–865 (1996).

15. Callamaras, N., Marchant, J. S., Sun, X.-P. & Parker, I. Activation and co-ordination of InsP3-mediated elementary Ca2+ events during global Ca2+ signals in Xenopus oocytes. *J. Physiol.* **509**, 81–91 (1998).

16. Dawson, S. P., Keizer, J. & Pearson, J. E. Fire– diffuse–fire model of dynamics of intracellular calcium waves. *Biochemistry* **96**, 6060–6063 (1999).

17. Marchant, J. S. & Parker, I. Role of elementary Ca2+ puffs in generating repetitive Ca2+ oscillations. *EMBO J.* **20**, 65–76 (2001).

18. Marchant, J., Callamaras, N. & Parker, I. Initiation of IP3-mediated Ca2+ waves in Xenopus oocytes. *EMBO J.* **18**, 5285–5299 (1999).

19. Rückl, M. & Rüdiger, S. Calcium waves in a grid of clustered channels with synchronous IP3 binding and unbinding. *Eur. Phys. J. E* **39**, 108 (2016).

20. Miyamoto, A. & Mikoshiba, K. A novel multi lines analysis tool of Ca2+ dynamics reveals the nonuniformity of Ca2+ propagation. *Cell Calcium* **78**, 76–80 (2019).
21. Sneyd, J. *et al.* Modeling calcium waves in an anatomically accurate three-dimensional parotid acinar cell. *J. Theor. Biol.* **419**, 383–393 (2017).
22. Sneyd, J. *et al.* On the dynamical structure of calcium oscillations. *Proc. Natl. Acad. Sci.* **114**, 1456 LP – 1461 (2017).
23. Rückl, M. *et al.* Modulation of Elementary Calcium Release Mediates a Transition from Puffs to Waves in an IP3R Cluster Model. *PLOS Comput. Biol.* **11**, e1003965 (2015).
24. Piegari, E., Villarruel, C. & Ponce Dawson, S. Changes in Ca2+ Removal Can Mask the Effects of Geometry During IP3R Mediated Ca2+ Signals. *Front. Physiol.* **10**, 964 (2019).
25. Mataragka, S. & Taylor, C. W. All three IP3 receptor subtypes generate Ca2+ puffs, the universal building blocks of IP3-evoked Ca2+ signals. *J. Cell Sci.* (2018) doi:10.1242/jcs.220848.
26. Ellefsen, K. L., Lock, J. T., Settle, B., Karsten, C. A. & Parker, I. Applications of FLIKA, a Python-based image processing and analysis platform, for studying local events of cellular calcium signaling. *Biochim. Biophys. Acta - Mol. Cell Res.* **1866**, 1171–1179 (2019).
27. Dargan, S. L. & Parker, I. Buffer kinetics shape the spatiotemporal patterns of IP3-evoked Ca2+ signals. *J. Physiol.* **553**, 775–788 (2003).
28. Smith, I. F., Wiltgen, S. M. & Parker, I. Localization of puff sites adjacent to the

plasma membrane: functional and spatial characterization of Ca2+ signaling in SH-SY5Y cells utilizing membrane-permeant caged IP3. *Cell Calcium* **45**, 65–76 (2009).

29. Swaminathan, D., Dickinson, G. D., Demuro, A. & Parker, I. Noise analysis of cytosolic calcium image data. *Cell Calcium* **86**, 102152 (2020).

30. Alzayady, K. J. *et al.* Defining the stoichiometry of inositol 1,4,5-trisphosphate binding required to initiate Ca2+ release. *Sci. Signal.* **9**, 1–12 (2016).

31. Dakin, K. & Li, W.-H. Cell membrane permeable esters of d-myo-inositol 1,4,5-trisphosphate. *Cell Calcium* **42**, 291–301 (2007).

32. Keebler, M. V. & Taylor, C. W. Endogenous signalling pathways and caged IP3 evoke Ca2+ puffs at the same abundant immobile intracellular sites. *J. Cell Sci.* **130**, 3728–3739 (2017).

33. Lock, J. T., Smith, I. F. & Parker, I. Comparison of Ca2+ puffs evoked by extracellular agonists and photoreleased IP3. *Cell Calcium* **63**, 43–47 (2017).

34. Rizzuto, R., De Stefani, D., Raffaello, A. & Mammucari, C. Mitochondria as sensors and regulators of calcium signalling. *Nat. Rev. Mol. Cell Biol.* **13**, 566 (2012).

35. Mammucari, C. *et al.* Mitochondrial calcium uptake in organ physiology: from molecular mechanism to animal models. *Pflügers Arch. - Eur. J. Physiol.* **470**, 1165–1179 (2018).

36. Morgan, A. J., Platt, F. M., Lloyd-Evans, E. & Galione, A. Molecular mechanisms of endolysosomal Ca2+ signalling in health and disease. *Biochem. J.* **439**, 349–378 (2011).

37. Yang, J. Release and uptake mechanisms of vesicular Ca2+ stores. *Protein Cell* **10**, 8–19 (2019).

38. Stout, A. K., Raphael, H. M., Kanterewicz, B. I., Klann, E. & Reynolds, I. J. Glutamate-induced neuron death requires mitochondrial calcium uptake. *Nat. Neurosci.* **1**, 366–373 (1998).

39. Jensen, J. R. & Rehder, V. FCCP releases Ca2+ from a non-mitochondrial store in an identifiedHelisoma neuron. *Brain Res.* **551**, 311–314 (1991).

40. Churchill, G. C. *et al.* NAADP Mobilizes Ca2+ from Reserve Granules, Lysosome-Related Organelles, in Sea Urchin Eggs. *Cell* **111**, 703–708 (2002).

41. Uyama, Y., Imaizumi, Y. & Watanabe, M. Effects of cyclopiazonic acid, a novel Ca2+-ATPase inhibitor, on contractile responses in skinned ileal smooth muscle. *Br. J. Pharmacol.* **106**, 208–214 (1992).

42. Lock, J. T., Alzayady, K. J., Yule, D. I. & Parker, I. All three IP3 receptor isoforms generate Ca2+ puffs that display similar characteristics. *Sci. Signal.* **11**, eaau0344 (2018).

43. Ellefsen, K. L. & Parker, I. Dynamic Ca2+ imaging with a simplified lattice light-sheet microscope: A sideways view of subcellular Ca2+ puffs. *Cell Calcium* **71**, 34–44 (2018).

44. Thillaiappan, N. B., Chavda, A. P., Tovey, S. C., Prole, D. L. & Taylor, C. W. Ca2+ signals initiate at immobile IP3 receptors adjacent to ER-plasma membrane junctions. *Nat. Commun.* **8**, 1505 (2017).

45. Yamasaki-Mann, M., Demuro, A. & Parker, I. Cytosolic [Ca2+] regulation of InsP3-evoked puffs. *Biochem. J.* **449**, 167 LP – 173 (2013).

46. Bootman, M., Niggli, E., Berridge, M. & Lipp, P. Imaging the hierarchical Ca2+ signalling system in HeLa cells. *J. Physiol.* **499**, 307–314 (1997).
47. Shuai, J., Pearson, J. E. & Parker, I. Modeling Ca2+ feedback on a single inositol 1,4,5-trisphosphate receptor and its modulation by Ca2+ buffers. *Biophys. J.* **95**, 3738–3752 (2008).
48. Wiltgen, S. M., Dickinson, G. D., Swaminathan, D. & Parker, I. Termination of calcium puffs and coupled closings of inositol trisphosphate receptor channels. *Cell Calcium* **56**, 157–168 (2014).
49. Stern, M. D., Ríos, E. & Maltsev, V. A. Life and death of a cardiac calcium spark. *J. Gen. Physiol.* **142**, 257 LP – 274 (2013).
50. Okubo, Y. *et al.* Visualization of Ca2+ Filling Mechanisms upon Synaptic Inputs in the Endoplasmic Reticulum of Cerebellar Purkinje Cells. *J. Neurosci.* **35**, 15837 LP – 15846 (2015).
51. Park, M. K., Petersen, O. H. & Tepikin, A. V. The endoplasmic reticulum as one continuous Ca2+ pool: visualization of rapid Ca2+ movements and equilibration. *EMBO J.* **19**, 5729–5739 (2000).
52. Smith, I. F., Swaminathan, D., Dickinson, G. D. & Parker, I. Single-Molecule Tracking of Inositol Trisphosphate Receptors Reveals Different Motilities and Distributions. *Biophys. J.* **107**, 834–845 (2014).
53. Tateishi, Y. *et al.* Cluster Formation of Inositol 1,4,5-Trisphosphate Receptor Requires Its Transition to Open State. *J. Biol. Chem.* **280**, 6816–6822 (2005).
54. Gibson, C. J. & Ehrlich, B. E. Inositol 1,4,5-trisphosphate receptor movement is restricted by addition of elevated levels of O-linked sugar. *Cell Calcium* **43**,

228–235 (2008).

55. Ferreri-Jacobia, M., Mak, D.-O. D. & Foskett, J. K. Translational Mobility of the Type 3 Inositol 1,4,5-Trisphosphate Receptor Ca2+ Release Channel in Endoplasmic Reticulum Membrane. *J. Biol. Chem.* **280**, 3824–3831 (2005).

56. Fukatsu, K. *et al.* Lateral Diffusion of Inositol 1,4,5-Trisphosphate Receptor Type 1 Is Regulated by Actin Filaments and 4.1N in Neuronal Dendrites. *J. Biol. Chem.* **279**, 48976–48982 (2004).

57. Dargan, S. L., Schwaller, B. & Parker, I. Spatiotemporal patterning of IP3-mediated Ca2+ signals in Xenopus oocytes by Ca2+-binding proteins. *J. Physiol.* **556**, 447–461 (2004).

58. Prole, D. L. & Taylor, C. W. Inositol 1,4,5-trisphosphate receptors and their protein partners as signalling hubs. *J. Physiol.* **594**, 2849–2866 (2016).

59. Lock, J. T., Smith, I. F. & Parker, I. Spatial-temporal patterning of Ca2+ signals by the subcellular distribution of IP3 and IP3 receptors. *Semin. Cell Dev. Biol.* **94**, 3–10 (2019).

60. Konieczny, V., Keebler, M. V & Taylor, C. W. Spatial organization of intracellular Ca2+ signals. *Semin. Cell Dev. Biol.* **23**, 172–180 (2012).

61. Thomas, A. P., Bird, G. S., Hajnoczky, G., Robb-Gaspers, L. D. & Putney, J. W. J. Spatial and temporal aspects of cellular calcium signaling. *FASEB J. Off. Publ. Fed. Am. Soc. Exp. Biol.* **10**, 1505–1517 (1996).

62. Dolmetsch, R. E., Xu, K. & Lewis, R. S. Calcium oscillations increase the efficiency and specificity of gene expression. *Nature* **392**, 933 (1998).

63. Li, W., Llopis, J., Whitney, M., Zlokarnik, G. & Tsien, R. Y. Cell-permeant caged

InsP3 ester shows that Ca2+ spike frequency can optimize gene expression. *Nature* **392**, 936–941 (1998).

64. Dupont, G., Combettes, L., Bird, G. S. & Putney, J. W. Calcium oscillations. *Cold Spring Harb. Perspect. Biol.* **3**, 10.1101/cshperspect.a004226 a004226 (2011).

65. Berridge, M. J., Bootman, M. D. & Roderick, H. L. Calcium signalling: dynamics, homeostasis and remodelling. *Nat. Rev. Mol. Cell Biol.* **4**, 517–529 (2003).

66. Thul, R., Bellamy, T. C., Roderick, H. L., Bootman, M. D. & Coombes, S. Calcium Oscillations BT - Cellular Oscillatory Mechanisms. in (eds. Maroto, M. & Monk, N. A. M.) 1–27 (Springer New York, 2009). doi:10.1007/978-0-387-09794-7_1.

67. Allbritton, N. L., Meyer, T. & Stryer, L. Range of messenger action of calcium-ion and inositol 1, 4, 5-trisphosphate. *Science (80-.).* **258**, 1812–1815 (1992).

68. Schwaller, B. Cytosolic Ca(2+) Buffers. *Cold Spring Harb. Perspect. Biol.* **2**, a004051 (2010).

69. Samanta, K. & Parekh, A. B. Spatial Ca2+ profiling: decrypting the universal cytosolic Ca2+ oscillation. *J. Physiol.* **595**, 3053–3062 (2017).

70. Atakpa, P., Thillaiappan, N. B., Mataragka, S., Prole, D. L. & Taylor, C. W. IP3 Receptors Preferentially Associate with ER-Lysosome Contact Sites and Selectively Deliver Ca2+ to Lysosomes. *Cell Rep.* **25**, 3180-3193.e7 (2018).

71. Csordás, G. *et al.* Imaging Interorganelle Contacts and Local Calcium Dynamics at the ER-Mitochondrial Interface. *Mol. Cell* **39**, 121–132 (2010).

72. Thillaiappan, N. B., Chakraborty, P., Hasan, G. & Taylor, C. W. IP3 receptors and Ca2+ entry. *Biochim. Biophys. Acta - Mol. Cell Res.* **1866**, 1092–1100 (2019).

73. Taylor, C. W. & Machaca, K. IP3 receptors and store-operated Ca2+ entry: a license to fill. *Curr. Opin. Cell Biol.* **57**, 1–7 (2019).

74. Giorgi, C., De Stefani, D., Bononi, A., Rizzuto, R. & Pinton, P. Structural and functional link between the mitochondrial network and the endoplasmic reticulum. *Int. J. Biochem. Cell Biol.* **41**, 1817–1827 (2009).

75. Filadi, R. & Pozzan, T. Generation and functions of second messengers microdomains. *Cell Calcium* **58**, 405–414 (2015).

76. Cárdenas, C. *et al.* Essential Regulation of Cell Bioenergetics by Constitutive InsP3 Receptor Ca2+ Transfer to Mitochondria. *Cell* **142**, 270–283 (2010).

77. Ellefsen, K. L., Settle, B., Parker, I. & Smith, I. F. An algorithm for automated detection, localization and measurement of local calcium signals from camera-based imaging. *Cell Calcium* **56**, 147–156 (2014).

1140

1141 **FIGURES**

1142 **Fig. 1**

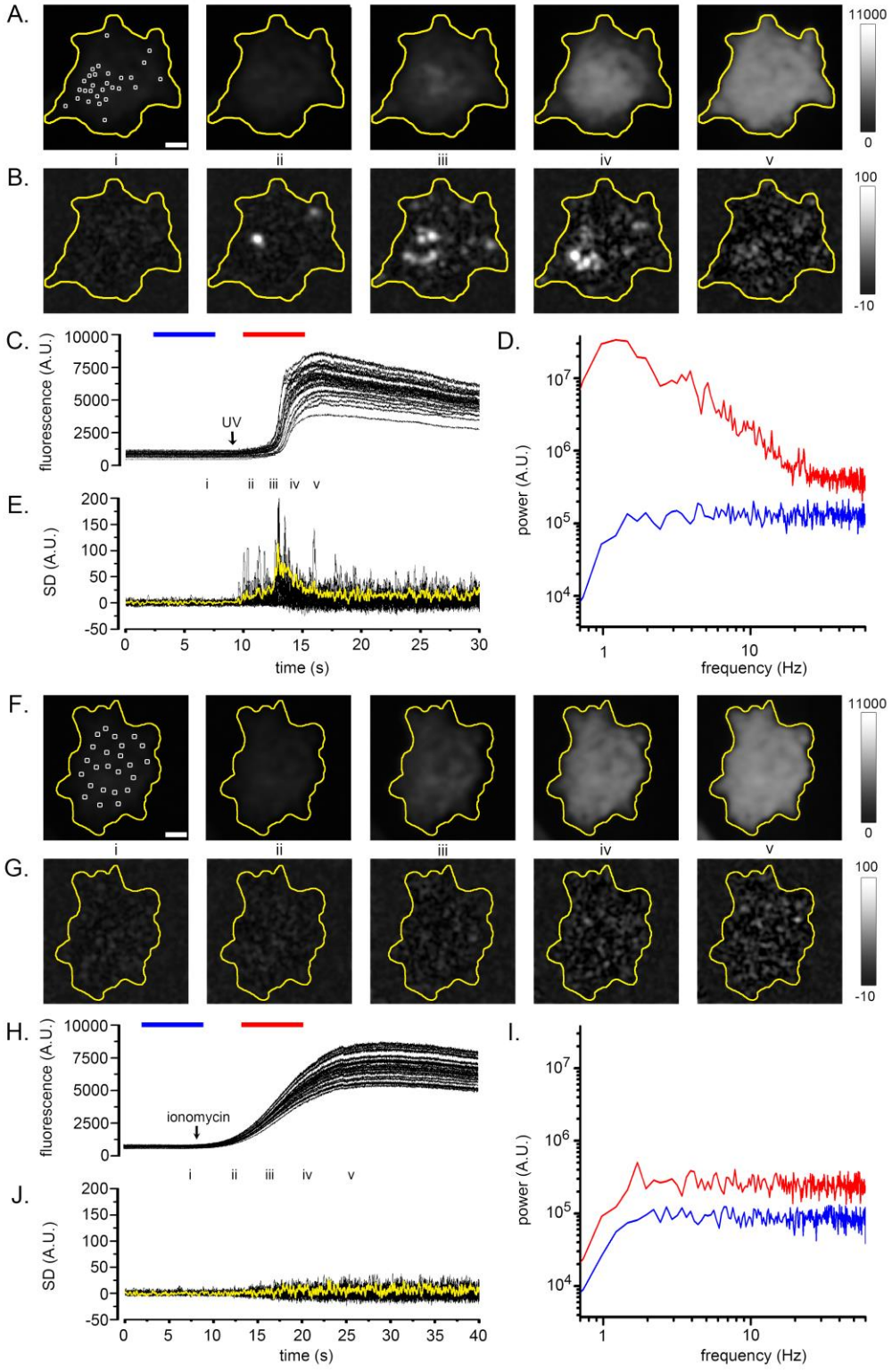

1143

Fig. 1. **Fluctuation analysis of Ca^{2+} signals. (A-D)** Records from a single WT HEK cell loaded with Cal520 and stimulated by photorelease of i-IP_3 to evoke a global Ca^{2+} elevation. **(A)** Panels show 'raw' TIRF fluorescence images of the cell before (i), during the rising phase (ii-iv) and at the peak (v) of the global Ca^{2+} signal. Images are Gaussian-blurred (sigma ~1 μm) single frames (8 ms exposure time) captured at times as marked in C. Grey scale intensities depict fluorescence in arbitrary camera units, as indicated by the bar at the right. The yellow outline marks the TIRF footprint of the cell. **(B)** Panels show corresponding standard deviation (SD) images at the same times as in A, highlighting hot spots of local, transient Ca^{2+} release. Grey scale intensities (arbitrary units; A.U.) represent the shot noise-corrected standard deviation of fluorescence fluctuations within a 160 ms running time window. **(C)** Overlaid black traces show fluorescence monitored from 24 regions of interest (ROIs; marked by squares in panel Ai) placed on areas of local Ca^{2+} activity. The arrow indicates the time of the photolysis flash. **(D)** Power spectra of Ca^{2+} fluorescence fluctuations averaged from the 24 ROIs at baseline (blue trace) and during the rising phase of the global Ca^{2+} signal (red trace). Spectra were calculated from recordings during the respective times indicated by the colored bars in C, after low-pass (1 Hz) filtering of the fluorescence image stack to strip out the slow rise of the global signal. **(E)** Overlaid traces show shot noise-corrected SD signals from the 24 ROIs centered on hot spots of Ca^{2+} activity. The thicker yellow trace shows the mean SD signal monitored from a ROI encompassing the entire cell and is depicted after scaling up by a factor of 10 relative to the traces from small ROIs. **(F-I)** Corresponding images and plots from an HEK cell devoid of IP_3Rs (3KO) in which a global Ca^{2+} elevation was evoked by pipetting a 10 μl aliquot of ionomycin into the bathing solution at a distance from the cell when marked by the arrow in H. In this case no hot spots or increased low frequency fluctuations accompanied the elevation in cytosolic [Ca^{2+}], and the ROIs (marked by squares in panel Fi) used to derive the

data in H-J were placed randomly. The yellow trace in J depicting the mean SD signal from the entire cell is scaled up by a factor of 10 relative to the traces from small ROIs. Fluorescence and SD magnitudes are expressed in arbitrary units consistent with those in A-D.

Fig. 2

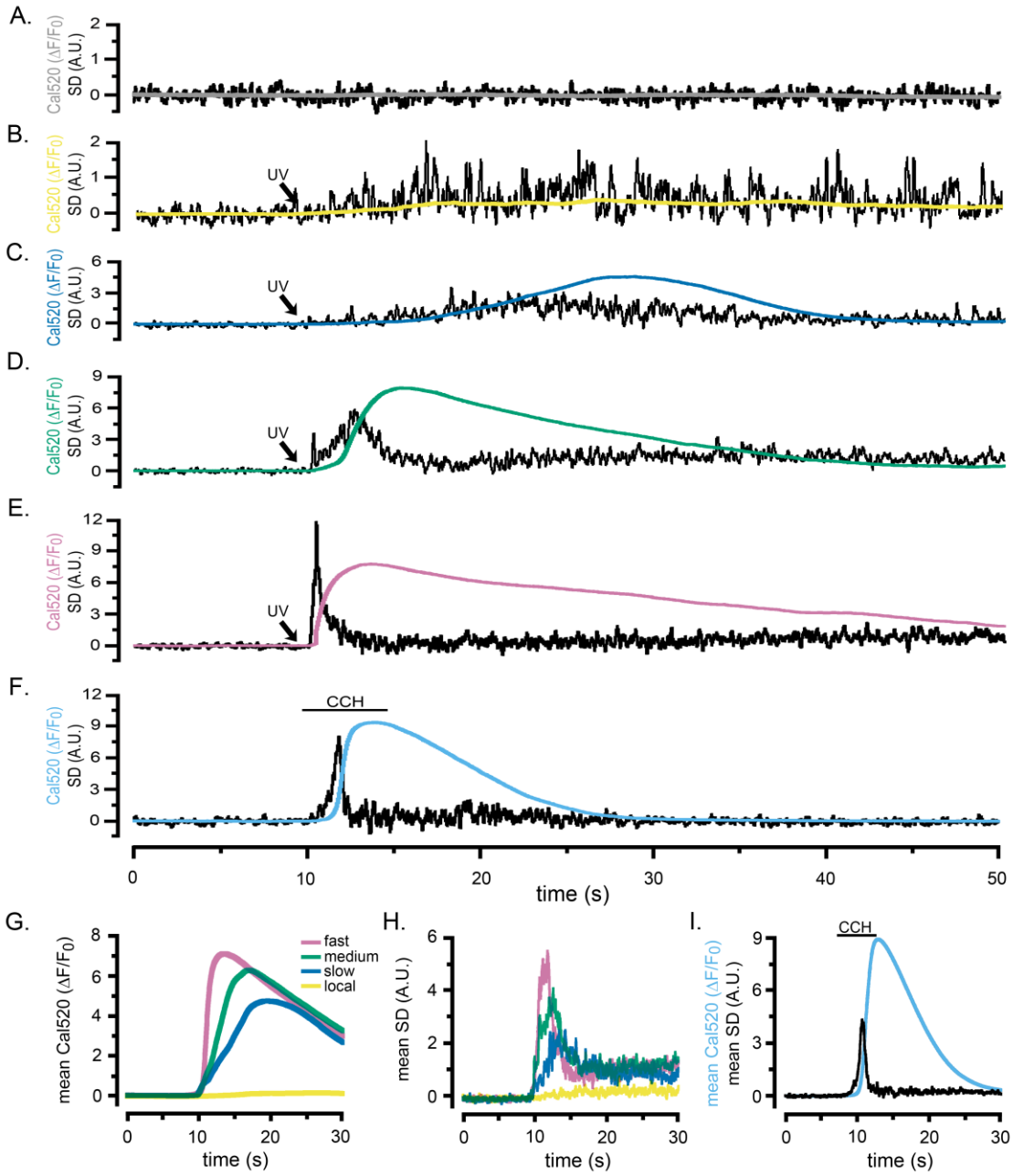
A.
B.
C.
D.
E.
F.
G.
H.
I.
Cal520 (ΔF/F0)
SD (A.U.)
UV
CCH
time (s)
mean Cal520 (ΔF/F0)
mean SD (A.U.)
fast
medium
slow
local

Fig. 2. Localized fluctuations in cytosolic [Ca^{2+}] occur predominantly during the rising phase of global Ca^{2+} elevations. Representative records show the Cal520 fluorescence ratio ($\Delta F/F_0$; smooth traces) and the associated SD fluctuation measurements (noisy traces) from ROIs encompassing single WT HEK cells bathed in Ca^{2+}-free medium. **(A)** Record obtained under basal conditions without stimulation. **(B-E)** Responses evoked by progressively longer photolysis flashes to release increasing amounts of i-IP_3 in cells loaded with caged i-IP_3. The SD signals are presented in arbitrary units (A.U.) but are consistent throughout all panels. To better display responses to weaker stimuli, the y-axes are scaled differently between panels. **(F)** Responses evoked by application of carbachol (CCH; 10 μM) when indicated by the bar. **(G, H)** Pooled data plotting, respectively, means of the global Ca^{2+} fluorescence signals and SD signals of cells stimulated with progressively increasing photorelease of i-IP_3 to evoke predominantly local Ca^{2+} signals (yellow traces; n=7), and global elevations with slow (blue; n=9), medium (green; n=13), and fast rising Ca^{2+} signals (pink; n=11). **(I)** Mean Cal520 fluorescence ratio signal (cyan trace) and SD signal (black trace) averaged from 12 cells stimulated by local application of 10 μM CCH when marked by the bar.

Fig. 3

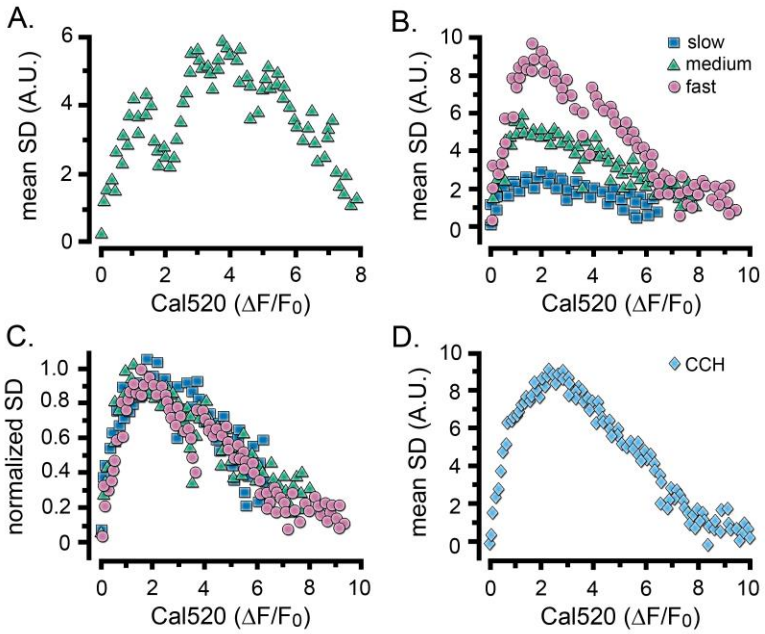

Fig. 3. Relationship between Ca^{2+} fluctuations and Ca^{2+} level during the rise of global Ca^{2+} signals. Scatter plots show measurements of the SD signal at intervals during the rising phase of global Ca^{2+} response against the magnitude of the global Ca^{2+} elevation ($\Delta F/F_0$) at that time. Data were binned at intervals of (0.1 $\Delta F/F_0$). **(A)** Measurements from the same cell as in Fig. 2D. **(B)** Data from the same groups of cells as in Fig. 2G,H, plotting mean SD signal amplitude as a function of mean Ca^{2+} level during global responses for cells exhibiting slow (blue squares), intermediate (green triangles) and fast rising responses (pink circles). **(C)** The same data as in B, after normalizing to the respective maximum SD signals for each group of cells. **(D)** Scatter plot of mean SD signal amplitude as a function of Ca^{2+} level during global responses for 12 cells stimulated by local application of CCH, as in Fig. 2I.

Fig. 4

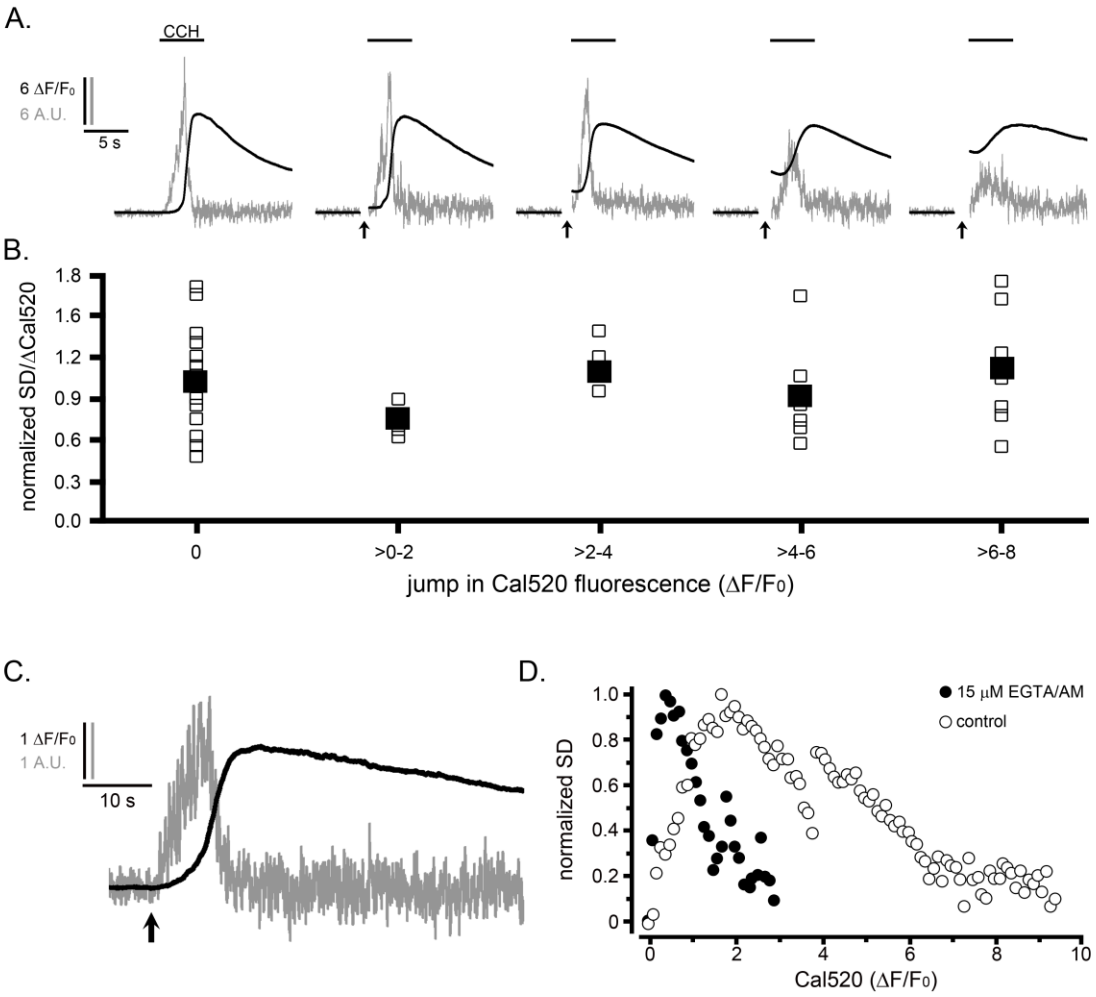

Fig. 4. The suppression of Ca^{2+} puffs during global signals does not result because of elevated cytosolic [Ca^{2+}]. (A,B) IP_3-evoked Ca^{2+} puffs are not suppressed by prior photorelease of Ca^{2+}. **(A)** Traces depict fluorescence ratios (black; $\Delta F/F_0$) from WT HEK cells and corresponding SD signals (grey; in arbitrary units, A.U.). Records, from left to right, show responses from individual cells loaded with NP-EGTA (caged Ca^{2+}) that were unstimulated or exposed to increasing UV flash durations (marked by arrows) to photorelease progressively increasing amounts of free Ca^{2+} before challenging cells with CCH (100 μM) locally delivered by a puffer pipette when indicated by the bars. Traces are

blanked out during the artifact caused by the photolysis flash. **(B)** Data points from traces like those in (A) show the integral under SD trace (a measure of puff activity) as a ratio of the change in global Ca^{2+} signal ($\Delta F/F_0$) evoked by CCH. The data are binned in terms of the jump in Cal520 fluorescence ($\Delta F/F_0$) evoked by photolysis of caged Ca^{2+}. Open symbols are from individual cells, and filled symbols are means for each group (respective n numbers for different bins; 20, 4, 4, 6, 8). Data are normalized with respect to the mean ratio without prior photorelease of Ca^{2+}. There was no significant difference between control CCH responses and CCH responses following Ca^{2+} jumps (evaluated by Student T-test; p values between 0.17 and 0.66 for the different binned groupings). **(C,D)** Termination of puff activity is unaffected when global cytosolic Ca^{2+} signals are attenuated by buffering with EGTA. **(C)** Traces showing the Cal520 fluorescence ratio ($\Delta F/F_0$; smooth trace) and SD signal (noisy trace) in response to photoreleased i-IP_3 in a representative WT HEK cell that was incubated with 15 μM EGTA/AM to buffer cytosolic Ca^{2+} and attenuate the amplitude of the global Ca^{2+} signal. **(D)** Scatter plots show measurements of the SD signal at intervals during the rising phase of global Ca^{2+} responses against the magnitude of the global Ca^{2+} elevation ($\Delta F/F_0$) at that time. Measurements were binned at intervals of (0.1 $\Delta F/F_0$) and SD data are normalized to a peak value of 1. Solid circles show mean data from 14 EGTA-loaded cells. For comparison, open circles present data reproduced from Fig. 3C showing measurements from 11 control cells that gave fast rising responses to photoreleased i-IP_3.

Fig. 5

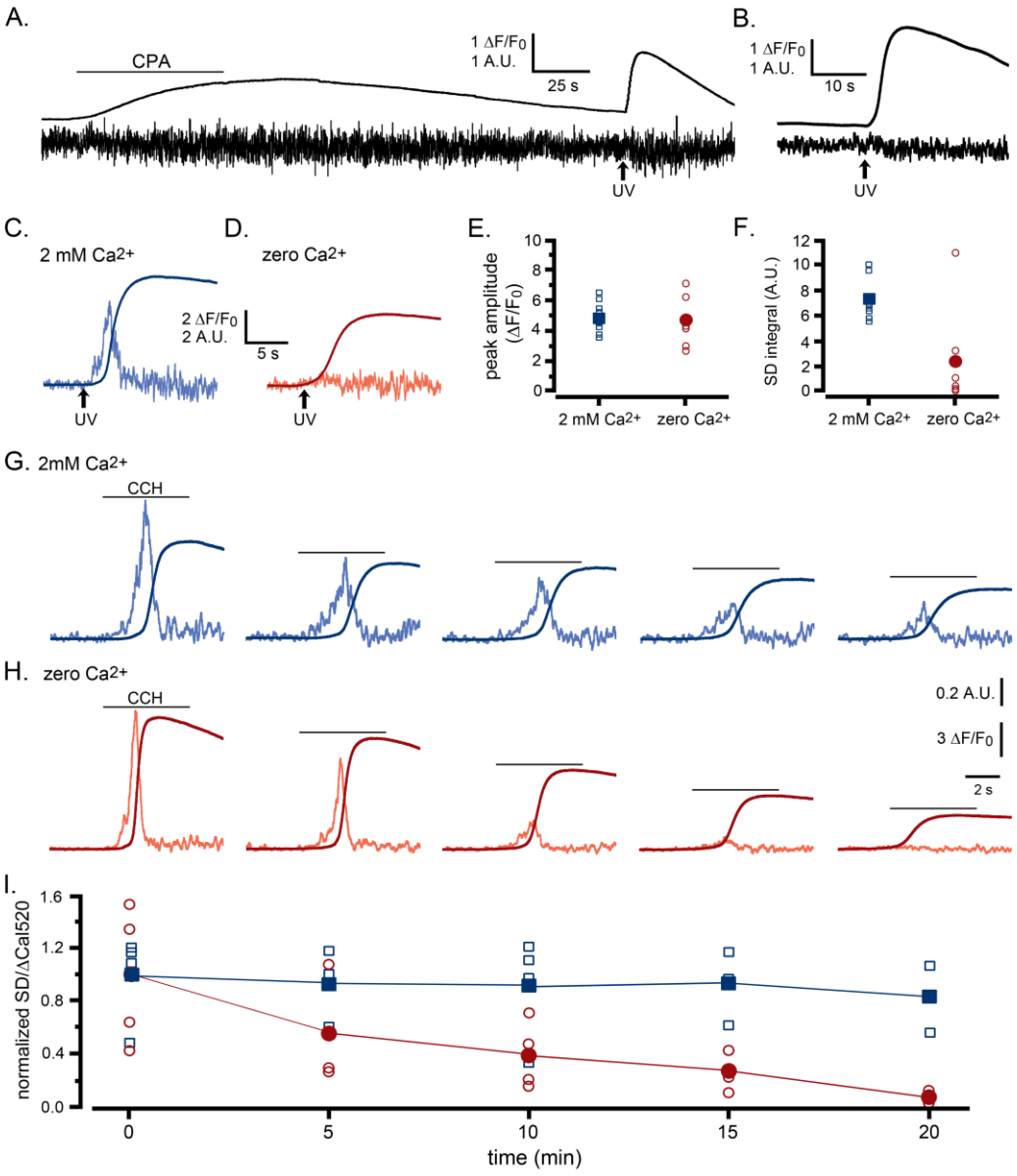

Fig. 5. Ca^{2+} puffs are selectively depressed by reduced ER Ca^{2+} content.

(A-F) Selective depression of puffs during i-IP_3-evoked global Ca^{2+} signals following depletion of ER Ca^{2+} content using transient application of cyclopiazonic acid (CPA; 50 μM) **(A)** The smooth trace shows fluorescence ratio ($\Delta F/F_0$) from a WT HEK cell, and the noisy trace the corresponding SD signal (in arbitrary units). The cell was bathed throughout in solution containing no added Ca^{2+} and 300 μM EGTA, and CPA was locally applied from a

puffer pipette during the time indicated by the bar. A UV flash was delivered when marked by the arrow to photorelease caged i-IP_3 loaded into the cell. **(B)** Mean $\Delta F/F_0$ and SD signals from 7 WT HEK cells in response to photoreleased i-IP_3 following CPA treatment and wash in Ca^{2+}-free medium as in A. **(C,D)** Representative $\Delta F/F_0$ and SD responses to photoreleased i-IP_3 in individual cells that were bathed, respectively, in Ca^{2+}-containing or Ca^{2+}-free medium for 30 min following treatment with CPA as in A. **(E)** Peak amplitudes of global fluorescence signals evoked by photoreleased i-IP_3 in experiments like those in C,D, for cells bathed in Ca^{2+}-containing (n = 8 cells; blue squares) or Ca^{2+}-free medium (n = 6; red circles). Open symbols denote measurements from individual cells; filled symbols are means. No significant difference between peak amplitudes ($\Delta F/F_0$) of cells bathed in Ca^{2+}-containing and Ca^{2+}-free medium (Student T test; p = 0.72). **(F)** Corresponding measurements of integral under SD traces (puff activity) during the time from the photolysis flash to the peak global fluorescence signal. SD integrals were significantly different between cells bathed in Ca^{2+}-containing and Ca^{2+}-free medium (Student T test; p = 0.012). **(G-I)** Selective depression of puffs by depleting ER Ca^{2+} content by repeated applications of CCH in zero Ca^{2+} bathing solution. **(G,H)** Global Ca^{2+} signals (smooth traces; $\Delta F/F_0$) and SD signals (noisy traces) evoked by successive, identical applications of CCH at 5 min intervals in two representative cells bathed, respectively, in medium containing 2 mM Ca^{2+} or 300 μM EGTA with no added Ca^{2+}. Amplitudes of the SD signals are depicted after normalizing to the peak amplitude of the first response for each cell. **(I)** Data points show the ratio of puff activity (integral under the SD trace) vs. peak magnitude of the global Ca^{2+} signal ($\Delta F/F_0$) for successive responses evoked by CCH application at 5 min intervals. Blue squares are data from cells bathed in medium containing 2 mM Ca^{2+} and red circles are from cells in Ca^{2+}-free medium; open symbols are ratios from individual cells and filled symbols are means. Data are plotted after normalizing to the mean SD integral and peak $\Delta F/F_0$ evoked by the initial stimulus in each

condition. Responses were significantly different between cells bathed in the presence and absence of external Ca^{2+} for times ≥ 10 min (Student T test; $p = 0.000008$).

Fig. 6

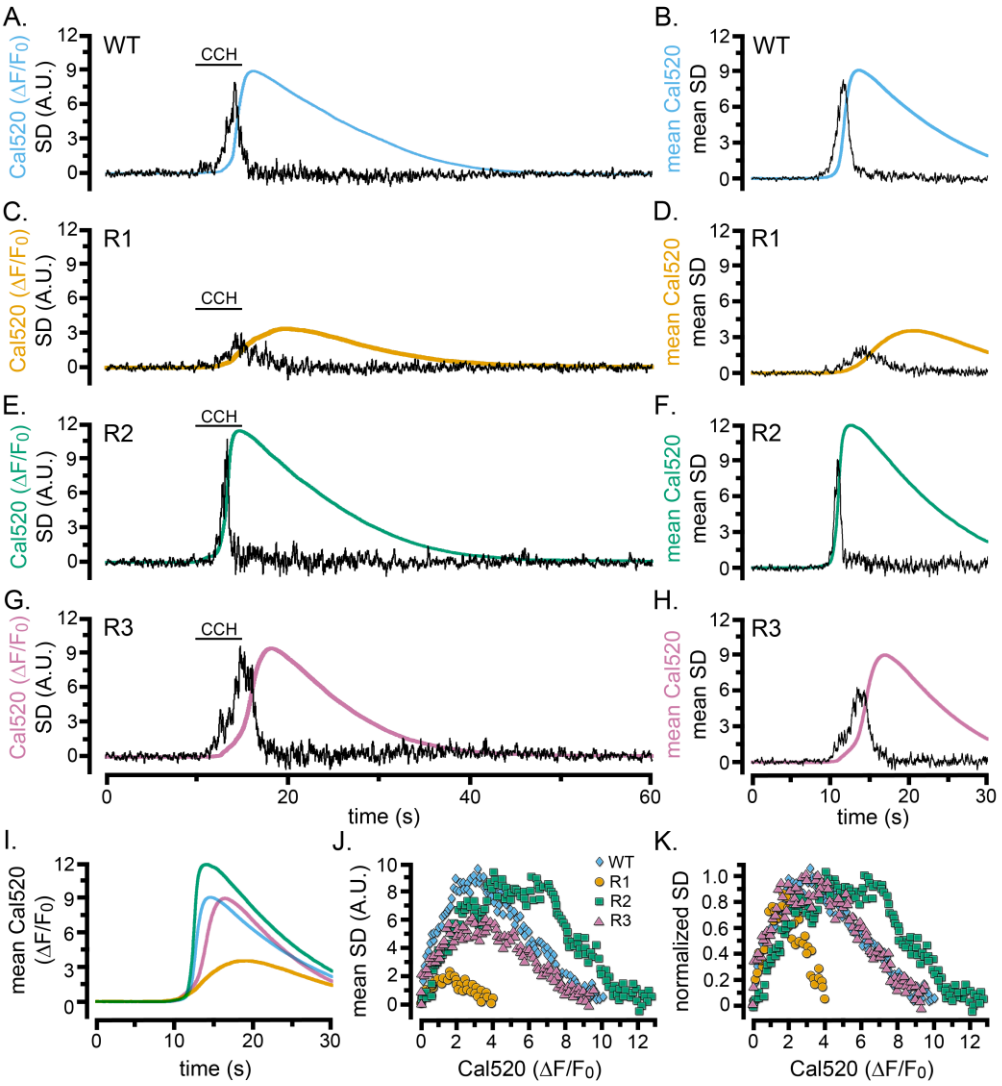

Fig. 6. Cell-wide Ca^{2+} elevations and SD fluctuations in WT HEK cells and cells exclusively expressing single IP_3R isoforms. **(A-H)** Traces show whole-cell Cal520 fluorescence ratio (smooth colored traces; $\Delta F/F_0$) and SD fluctuations (noisy black traces) of HEK cells locally stimulated with CCH locally delivered in a Ca^{2+}-containing bath solution when indicated by the bars. Panels on the left are representative records from individual cells, and panels on the right show mean traces from 7 (B) or 3 (D,F,H) cells. **(A,**

B) Records from HEK WT cells. **(C-H)** Records from HEK cells solely expressing IP_3R1 (C,D), IP_3R2 (E,F), or IP_3R3 (G,H). **(I)** Overlaid mean Cal520 fluorescence ratio traces, aligned to their rising phase, in WT HEK cells (cyan; n=7), and HEK cells solely expressing IP_3R1 (gold; n=3), IP_3R2 (green; n=3), and IP_3R3 (pink; n=3). **(J)** Scatter plots of SD signal vs. fluorescence ratio during the rising phase of the Ca^{2+} responses in WT HEK cells (cyan diamonds) and HEK cells solely expressing IP_3R1 (gold circles) IP_3R2 (green squares) or IP_3R3 (pink triangles). Data points are means from the same cells as in I. **(K)** The same data as in J, after normalizing to the same peak SD values.

Fig. 7

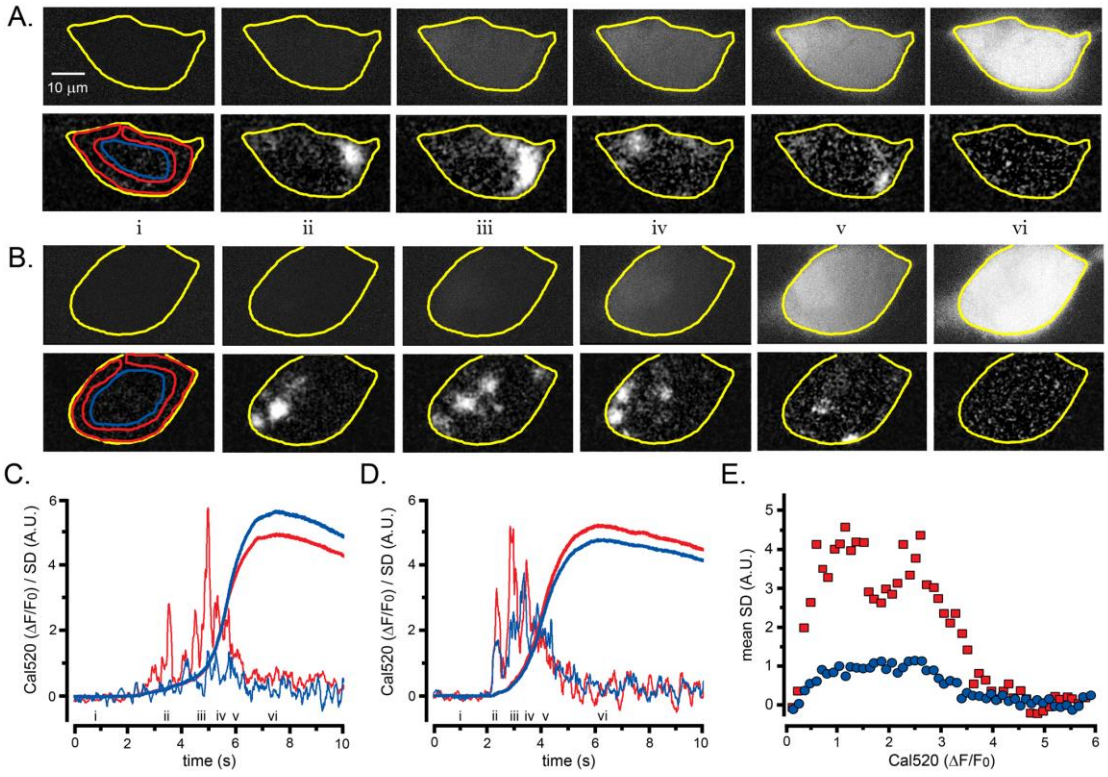

Fig. 7. Lightsheet imaging of global Ca^{2+} elevations evoked in HEK cells by photoreleased i-IP_3. **(A)** Upper panels show 45° diagonal image 'slices' through the center of a WT HEK cell imaged by lattice light-sheet microscopy. Grey scale intensities correspond to increases in fluorescence (ΔF) of Cal520 relative to the mean intensity (F_0) averaged over 100 frames before stimulation ($\Delta F/F_0$). Each panel is a single 10 ms exposure, captured at times before and after stimulation, as indicated by the Roman numerals in C. The cell outline is marked in yellow. Lower panels show corresponding SD images, at times corresponding to the upper panels. Colored outlines mark ROIs used to derive $\Delta F/F_0$ and SD traces from peripheral (red) and center (blue) regions of the cell. **(B)** Corresponding $\Delta F/F_0$ and SD lightsheet images from a different HEK cell that showed more prominent puff activity in the center of the cell. **(C)** Measurements of $\Delta F/F_0$ (smooth traces)

and SD (noisy traces) from the cell illustrated in A. Traces in red show average measurements from the peripheral region of interest marked in the bottom left panel of A, and traces in blue show measurements from the central region of interest. **(D)** Corresponding measurements of $\Delta F/F_0$ and SD from the cell illustrated in B. **(E)** Scatter plot of SD signal versus Ca^{2+} fluorescence ($\Delta F/F_0$) at intervals during the rising phase of global Ca^{2+} signals. Data are mean ±1 sem from 8 cells, with measurements binned at intervals of 0.1 $\Delta F/F_0$.

Fig. 8

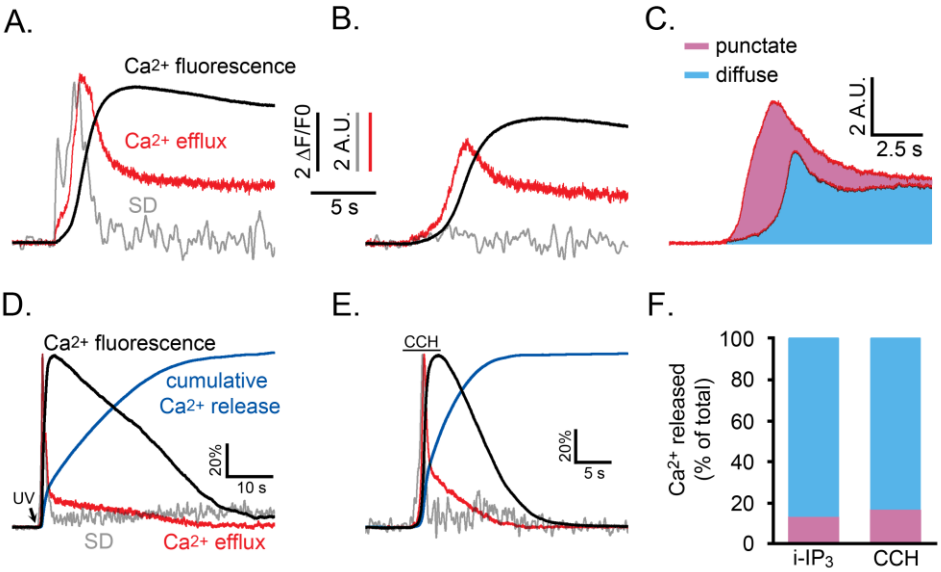

Fig. 8. Relative proportions of Ca^{2+} released by punctate versus diffuse modes of Ca^{2+} liberation during an IP_3-evoked global Ca^{2+} signal. **(A,B)** Whole cell Ca^{2+} fluorescence responses (black traces) and associated SD signals (grey traces) during the initial phase of a Ca^{2+} response evoked by photoreleased i-IP_3 in representative WT HEK cells. The red traces show the estimated rate of Ca^{2+} efflux, derived as described in the text. Both panels show responses from cells pretreated with CPA as in Fig. 5A that were treated identically, except that the cell in A was incubated in Ca^{2+}-containing medium to allow refilling of ER Ca^{2+} whereas the cell in B was incubated in Ca^{2+}-free medium to maintain the ER Ca^{2+} in a partially depleted state and suppress puff activity. The SD and Ca^{2+} efflux traces in A are scaled to similar peak height for clarity; traces in B are scaled the same as in A. **(C)** Mean Ca^{2+} efflux traces from 5 cells in Ca^{2+}-containing medium that showed robust puff activity (top) and 6 cells in Ca^{2+}-free medium where puff activity was almost absent (lower). The area shaded blue reflects the relative amount of Ca^{2+} released when puff activity was absent, and the pink area reflects the additional amount of Ca^{2+} release attributable to Ca^{2+}

puffs. **(D,E)** Traces show SD signal (grey), global Ca^{2+} fluorescence ratio (black) and calculated Ca^{2+} efflux rate (red) for the entire duration of responses evoked by photoreleased i-IP_3 **(D)** and by CCH **(E)**. Blue traces additionally show the cumulative percentage of Ca^{2+} released, derived by integrating under the red Ca^{2+} efflux traces. For clarity of presentation all traces are shown scaled to the same peak height. **(F)** Bars show mean percentages of total Ca^{2+} release during i-IP_3-evoked (left; n = 8 cells) and CCH-evoked signals (right; n = 7 cells) under control conditions attributable to punctate (pink) and diffuse (blue) modes of Ca^{2+} liberation. Data were calculated from the cumulative Ca^{2+} release at the time puff activity had ceased in each cell, assuming 41% of that release was due to punctate release.